Magnetic Resonance Image Based Quantification of Ophthalmic Changes in Long-Duration Spaceflight Astronauts

A Thesis

Presented in Partial Fulfillment of the Requirements for the

Degree of Master of Science

with a

Major in Biological engineering

in the

College of Graduate Studies

University of Idaho

by

Jesse J. Rohr

Major Professor: Bryn A. Martin, Ph.D.

Committee Members: Nathan R. Schiele, Ph.D.; Russell Qualls, Ph.D.; Dev Shrestha, Ph.D.

Department Administrator: Ching-An Peng, Ph.D.

December 2019

Authorization to Submit Thesis

This thesis of Jesse Rohr, submitted for the degree of Master of Science with a major in Biological engineering and titled "Magnetic Resonance Image Based Quantification of Ophthalmic Changes in Long-Duration Spaceflight Astronauts", has been reviewed in final form. Permission, as indicated by the signatures and dates given below, is now granted to submit final copies to the College of Graduate Studies for approval.

Major Professor: _____ Date: _____
Bryn A. Martin, Ph.D.

Committee Members: _____ Date: _____
Nathan R. Schiele, Ph.D.

_____ Date: _____
Russell Qualls, Ph.D.

_____ Date: _____
Dev Shrestha, Ph.D.

Department Administrator: _____ Date: _____
Ching-An Peng, Ph.D.

Abstract

Extended visits to microgravity have resulted in many ophthalmic abnormalities in some long-duration spaceflight astronauts. In combination, these symptoms define the SANS. Theorized to be a result of increased intracranial pressure (ICP) due to headward fluid shifts, these issues often persist for some time after return to Earth and will likely worsen on extended spaceflight ventures such as visits to Mars. In particular, changes to the optic nerve (ON), optic nerve sheath (ONS), and the posterior optic globe may have an underlying impact on ocular function. The following studies provide reliable, automated, and quantitative analysis of ON and ONS tortuosity and cross-sectional area as well as volumetric globe deformation in long-duration spaceflight astronauts. High resolution MR images were collected pre-flight followed by five recovery timepoints post-flight for (n = 10) astronauts. These recovery scans extending to one year after return from 6-month missions to the international space station. Methods were developed, reliability tested, and applied to assess ON tortuosity, ON and ONS cross-sectional areas, and volumetric globe deformation in all subjects. There were no spaceflight associated changes in tortuosity or cross-sectional areas while changes to globe deformation were quantified. The average and percent change in tortuosity, ON area, ONS area, and volumetric globe deformation immediately post-flight was -0.06 ± 0.42 mm (-0.9%), 0.58 ± 2.53 mm^2 (6.7%), -0.88 ± 2.35 mm^2 (-3.7%), and 10.76 ± 11.93 mm^3 respectively. Tortuosity and ON/ONS area values at recovery timepoints were relatively consistent over time. Globe deformation values generally decreased across these timepoints indicating recovery after return to Earth. Quantitative highly automated MRI based

assessment of the ocular structures could help our understanding of SANS and assist its prevention.

Acknowledgments

I would like to thank my major professor Dr. Martin for his guidance throughout my involvement in his laboratory at the University of Idaho. His expertise and mentorship have been invaluable for my development as an engineer and as a student of life. Thank you for pushing me to reach my goals. I would also like to thank my committee members Dr. Schiele, Dr. Qualls, and Dr. Shrestha for their guidance and expertise in both my education and development of my thesis. Additionally, I would like to thank Dr. Macias, Dr. Marshall-Goebel, and Dr. Stenger from KBR Wyle Laboratories and NASA for their mentorship on this project. Their lifelong work in the industry has allowed for my involvement on this project. Thank you for involving me with this important work. Finally, I would like to thank all the faculty and staff of the Department of Biological Engineering at the University of Idaho for their friendly and supportive graduated experience.

This study was supported by funds from NASA Idaho Space Grant Consortium grant #NNX10AM75H, NASA grant #NNX16AT06G, and KBR Wyle.

Dedication

Thank you to my family for motivating and supporting me throughout my life. I could never repay my parents, Jeff and Janice Rohr, for the sacrifices they have made to offer me my education, a lifetime of wonderful memories, endless support, and a wonderful home to grow up in. I would also like to thank my grandparents, aunts and uncles, as well as all of my cousins for their continued support and love. Your continued support has motivated me to accomplish my goals throughout my life as well as here in graduate school.

Table of Contents

List of Figures

List of Tables

Statement of Contribution

Bryn Martin conceived of the presented idea and secured research funding for the work. Jesse Rohr led the overall presentation of results. Jesse Rohr, Austin Sass, and Bryn Martin developed the theory. Jesse Rohr and Austin Sass developed and scripted measurement parameters. Jesse Rohr, Austin Sass, and Stuart Sater performed analysis of all measurements and drafted manuscripts and figures. All authors provided critical feedback and commented on the manuscript.

Authors:

Jesse J. Rohr: Neurophysiological Imaging and Modeling Laboratory

University of Idaho, 875 Perimeter Dr. MC1122, Moscow, ID, 83844-1122, U.S.A.

Austin M. Sass: Neurophysiological Imaging and Modeling Laboratory

University of Idaho, 875 Perimeter Dr. MC1122, Moscow, ID, 83844-1122, U.S.A.

Stuart H. Sater: Neurophysiological Imaging and Modeling Laboratory

University of Idaho, 875 Perimeter Dr. MC1122, Moscow, ID, 83844-1122, U.S.A.

Karina Marshall Goebel: Johnson Space Center Cardiovascular and Vision Laboratory,

KBRwyle, Houston, TX

C. Ross Ethier: Wallace H. Coulter Department of Biomedical Engineering, Georgia Institute of

Technology and Emory University, Atlanta, GA

Michael B. Stenger: Johnson Space Center Cardiovascular and Vision Laboratory, National

Aeronautics and Space Administration, Houston, TX

Brandon Macias: Johnson Space Center Cardiovascular and Vision Laboratory, KBRwyle,

Houston, TX

Bryn A. Martin: Neurophysiological Imaging and Modeling Laboratory

University of Idaho, 875 Perimeter Dr. MC1122, Moscow, ID, 83844-1122, U.S.A.

Chapter 1: Background

Spending extended time in a microgravity environment has been known to cause many well documented issues within the human body. To counteract these issues NASA has composed a complete list of risks associated with extended spaceflight (Figure 1.1). Some of the more commonly discussed impacts of leaving our gravitational field are bone and muscular atrophy, radiation exposure, mental health impacts of isolation and confinement, and cardiovascular deconditioning. A more recent issue that has become a focus within the space community is the effect of extended spaceflight on the function and structure of the human eye. An overview of the current understanding of all these issues are presented here.

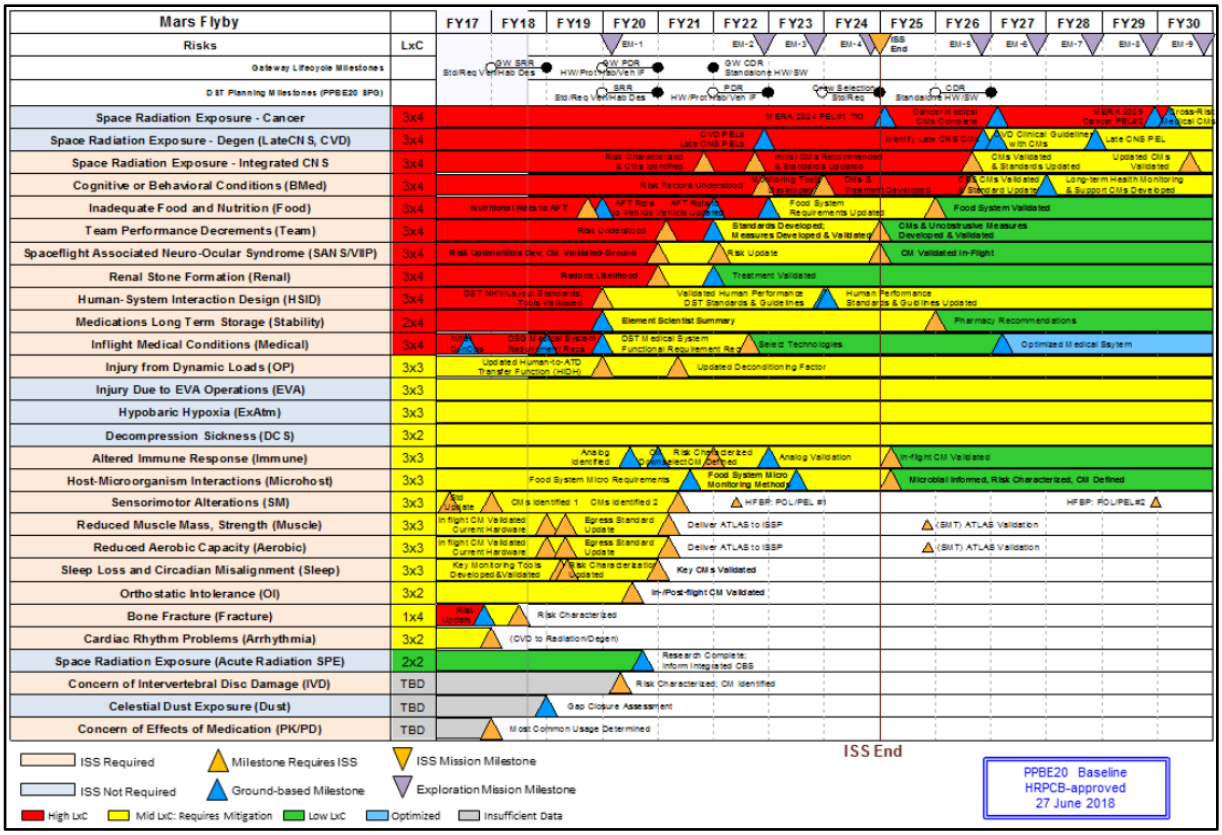

Figure 1.1. NASA HRP integrated path to risk reduction highlighting all current risks associated with long-duration spaceflight missions (figure from 1).

Skeletomuscular Atrophy

Without gravity to weigh us down our skeletomuscular system is required less, specifically in locations used to support body weight. Due to highly reduced activity in these regions, bone and muscle mass can rapidly reduce as a result of natural reabsorption of these tissues by the body. This reduction in tissue mass ultimately weakens these structures presenting structural issues upon return to Earth. Atrophy of these tissues were first noted in the 70's with human research conducted in Skylab[2]. Now research is more commonly conducted on rodents that share very similar DNA related to our skeletomuscular system. Changes in these rodents occur at a more rapid pace allowing us to estimate the effect of longer stays in microgravity on the human body. Muscle loss has been reported to be up to

20% in only a week and a half while bone loss is roughly 1.5% per month[3]. Currently out main countermeasure for avoiding muscle and bone atrophy is physical activity. Specially designed resistance equipment is utilized for multiple hours every day, in combination with highly controlled diets, to slow the tissue loss.

Ionizing Radiation Exposure

On earth we experience relatively small amounts of radiation every day from our sun and the surrounding space. This is usually in the form of low-energy non-ionizing radiation such as ultraviolet light, microwaves, and radio frequencies. The Earth's magnetic field and atmosphere play an essential role in protecting us from the bombardment of high-energy ionizing radiation. These include alpha particles, beta particles, gamma rays, and galactic cosmic rays from deep space. These particles can travel at velocities approaching the speed of light passing through and tearing apart any material in their way. While low earth orbits are not completely exposed to the full radiation of deep space, exposure is still significantly higher than on Earth. The radiation experienced by astronauts on missions to the international space station (ISS), moon, or Mars range from 50 to 2,000 millisieverts[4]. This is much higher than the annual radiation exposure on Earth of 6.2 millisieverts in the United States[5]. Astronauts on the ISS receive over ten times the radiation experienced on Earth which over time can lead to cancer as well as altered cognitive, motor, and behavioral functions[6]. Solar particle events, in which the sun releases large amounts of ionizing particles into space, are also a major concern for the health of astronauts.

Isolation and Confinement

Additionally, the constant isolation and confinement to very small spaces experienced by astronauts in microgravity impacts further on their mental health. Behavioral issues develop even with careful training and include changes in mood, cognition, morale, and interpersonal interactions[6]. These developments are major concerns for future missions that are further reaching from Earth. As a countermeasure, ISS mission astronauts maintain frequent contact with many people across the world including scientists, students, and mission control. Unfortunately, missions like the trip to Mars will not allow for real time communication. This, in combination with the associated extended duration and the further reduced size of living quarters of such a mission, raises concern for the mental wellbeing and critical decision making of astronauts.

Cardiovascular Deconditioning

Cardiovascular deconditioning also occurs in astronauts as a result of extended spaceflight. Due to the absence of our standard gravitation field the cardiovascular system will develop a number of changes including; resetting of carotid baroreceptors as well as decreases in circulating blood and interstitial fluids, arterial blood diastolic pressure, ventricular stroke volume, and left ventricular mass[7]. Generally, these changes do not negatively affect the person while still in microgravity as they are adaptation to the new physical state. However, upon return to Earth many effects may occur. These include hearth palpations, increased hearth rate, and reduced exercise capacity among others. As with most biological adaptations, extended visits to microgravity will likely equate to increased severity of these changes.

Headward Fluid Shift and Spaceflight Associated Neuro-Ocular Syndrome (SANS)

One prominent feature of cardiovascular adaptation is headward fluid shift which is likely to occur rapidly upon entering microgravity. Blood and cerebrospinal fluid (CSF) within the body move toward the head without the effects of gravity on the body (Figure 1.2). Natural mechanisms, that normally counteract gravity in order to maintain homeostasis within these systems, continue to occur within the body causing the headward flux of fluids. Because of this several changes and issues have been observed in the astronaut population specifically related to the softer tissues within the cranium that interface both with cerebrospinal fluid and blood. It is believed that these tissues are directly impacted either by the associated elevated intracranial pressure (ICP) or simply the remodeling of tissues under a differing physical state.

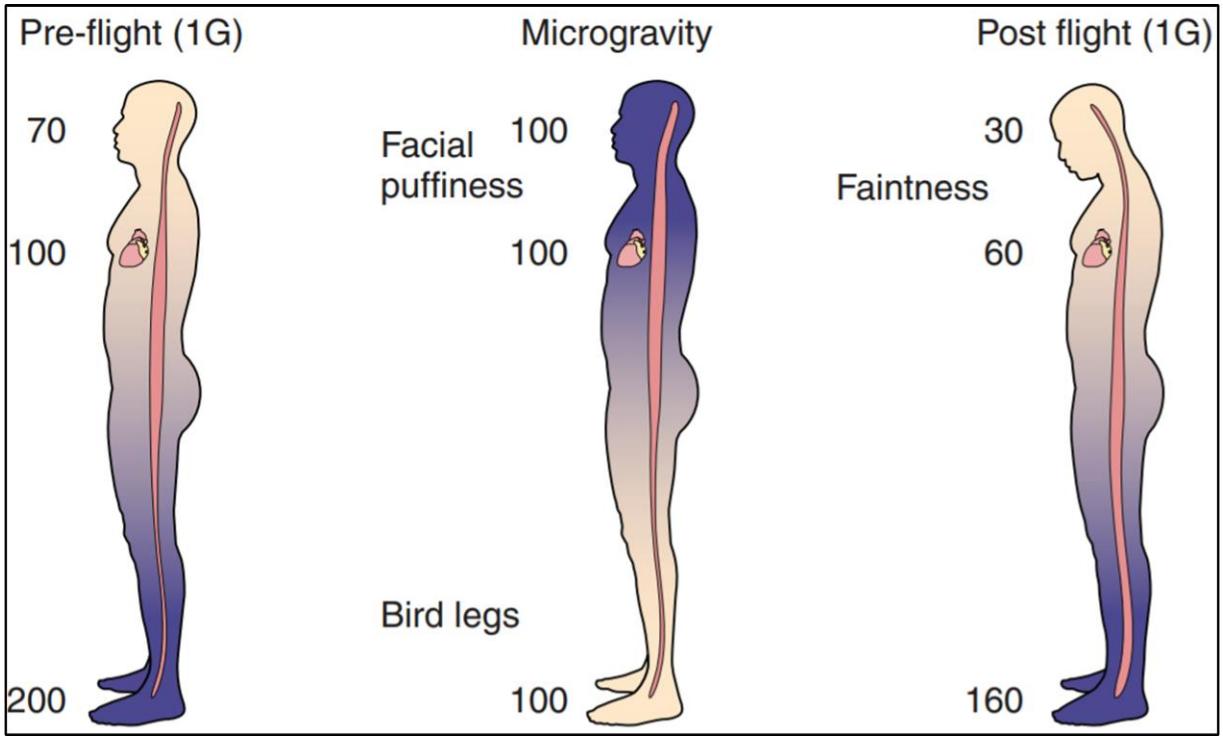

Figure 1.2. Microgravity induced fluid shifts and associated mean arterial pressures in mmHg. Blue shaded regions indicate locations of high tissue fluid (figure from 8).

In a study conducted by Roberts et al. long-duration spaceflight astronauts were observed to have a narrowing of the central sulcus of the brain, an upward shift of the brain, and a narrowing of the CSF space at the cranial vertex[9]. Albeit, the results from this study have been questioned by the research community for their level of accuracy and reproducibility. Each of these adaptations reflect the expected response to exiting our gravitational field. They don't appear to cause any issues with the astronauts though longer missions, such as a trip to Mars, may allow for further displacement of the brain and CSF. Further disturbances of these structures may possibly result in unforeseen issues.

In the same study by Roberts et al., astronauts on long-duration spaceflight missions were observed to have expansion of the ventricles[9]. This would be in relation to additional CSF within the cranium causing elevated ICP. Another report by Kramer et al. also found that

astronaut's total CSF ventricular volume was increased resulting from spaceflight and did not return to baseline values after a one-year period[10]. A terrestrial analog for this occurrence is hydrocephalus, which can result in brain damage and death. Additional fluid in the cranium causing elevated ICP would indicate the possibility of ventricle expansion however this occurrence is still debated.

In addition to the changes observed in the brain, many changes to the eye ON have been reported as well. The ON is surrounded by CSF and a thin sheath comprised of pia matter, arachnoid matter, and dura matter. Depending on the location along the ON varying types of connective tissues fill the subarachnoid space containing CSF (Figure 1.3). Pressure changes in these various segments affect the structure differently due to the varying connective tissues and geometries. The bulbar section of ON is particularly susceptible to structural change due to its larger size, thin trabeculae, and because the CSF within the subarachnoid space can only flow away from the globe. Due to headward fluid shifts and the influx of CSF into this space expansion of the bulbar segment has been observed in astronauts. This influx of CSF and blood to these tissues has caused several changes to the eye raising concern for astronaut ocular health and function.

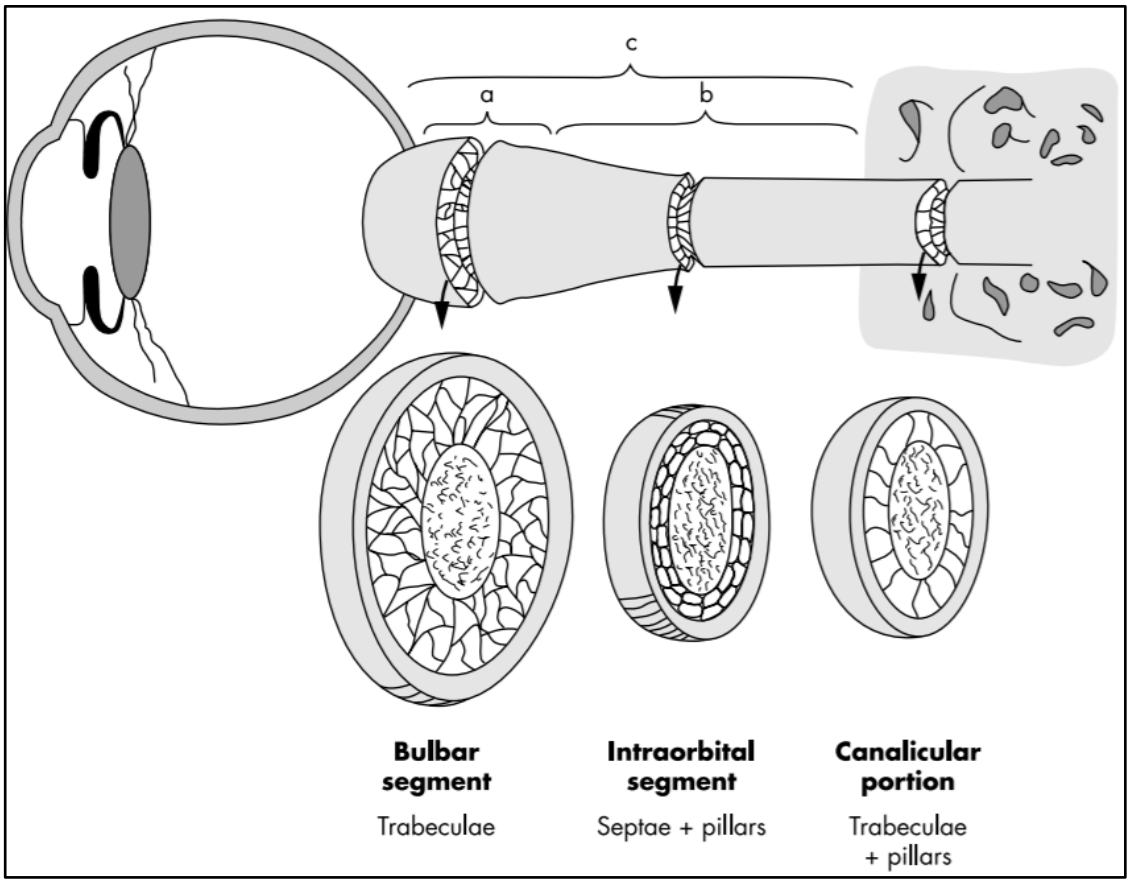

Figure 1.3. ON and ONS schematic showing a) bulbar segment containing trabeculae, b) mid-orbital segment containing septae and pillars, and c) canalicular portion containing pillars (figure from 11)

SANS describes the ophthalmic changes experienced by some astronauts as a result of headward fluid shifts. These changes include hyperopic shifts, optic disc edema, cotton wool spots, choroidal folds, and globe flattening. Often ON kinks have been observed in the astronaut population as well. It has been difficult to predict any of these conditions within the astronaut cohort. Likely due to the high degree of variation within the astronauts include age and sex as well as differing anatomical structures and fluid volumes, most cases of SANS are variant in degree of severity. Additionally, there is no clear pattern to symptom development within these individuals making the creation of countermeasures and the

prediction of SANS occurrence very difficult. Each of the reported symptoms of SANS are described in detail below.

Hyperopic Shifts

Hyperopic shift is a decrease in myopia which causes the focal point of light passing through the lens to land behind the retina. This causes a change in visual acuity and is experienced as blurry vision initially. Roughly 50% of astronauts experience a hyperopic shift and it is often associated with globe flattening where the position of the retina moves anteriorly toward the lens. A study by Mader et al. analyzing 7 long-duration spaceflight astronauts reported hyperopic shift of at least 0.5 diopters with a range of 0.5 ± 1.75 diopters in 5 (71%) of the subjects[12]. These changes were observed to occur within 3 weeks of exposure to microgravity. After returning to Earth this condition tends to correct itself however return missions can cause these changes to reoccur and worsen. Longer missions may prove to have lasting and possibly permanent effects.

Optic Disc Edema

Swelling of the optic disc (the location where the ON connects with the retina) as a result of increased fluid and pressure within, or surrounding, the axon can result in vision loss. Scanning laser ophthalmoscopy (SLO) or dilated fundus examinations (DFE) are performed on each subject to visualize the tissues at the posterior globe. DFE are frequently performed causing the pupil to enlarge allowing for a fundus camera to image the retina and ON head in high resolution and color. As with hyperopic shift, Mader et al. reported 5 of 7 long-duration

spaceflight astronauts developed optic disc edema. For these individuals disc swelling gradually resolved upon return to earth within a few weeks. However, one case study reported optic disc edema that persisted long after return for one long-duration space flight astronaut[13]. Additionally, asymmetric ocular changes were observed in this case study as well as in other long-duration spaceflight astronauts (Figure 1.4)

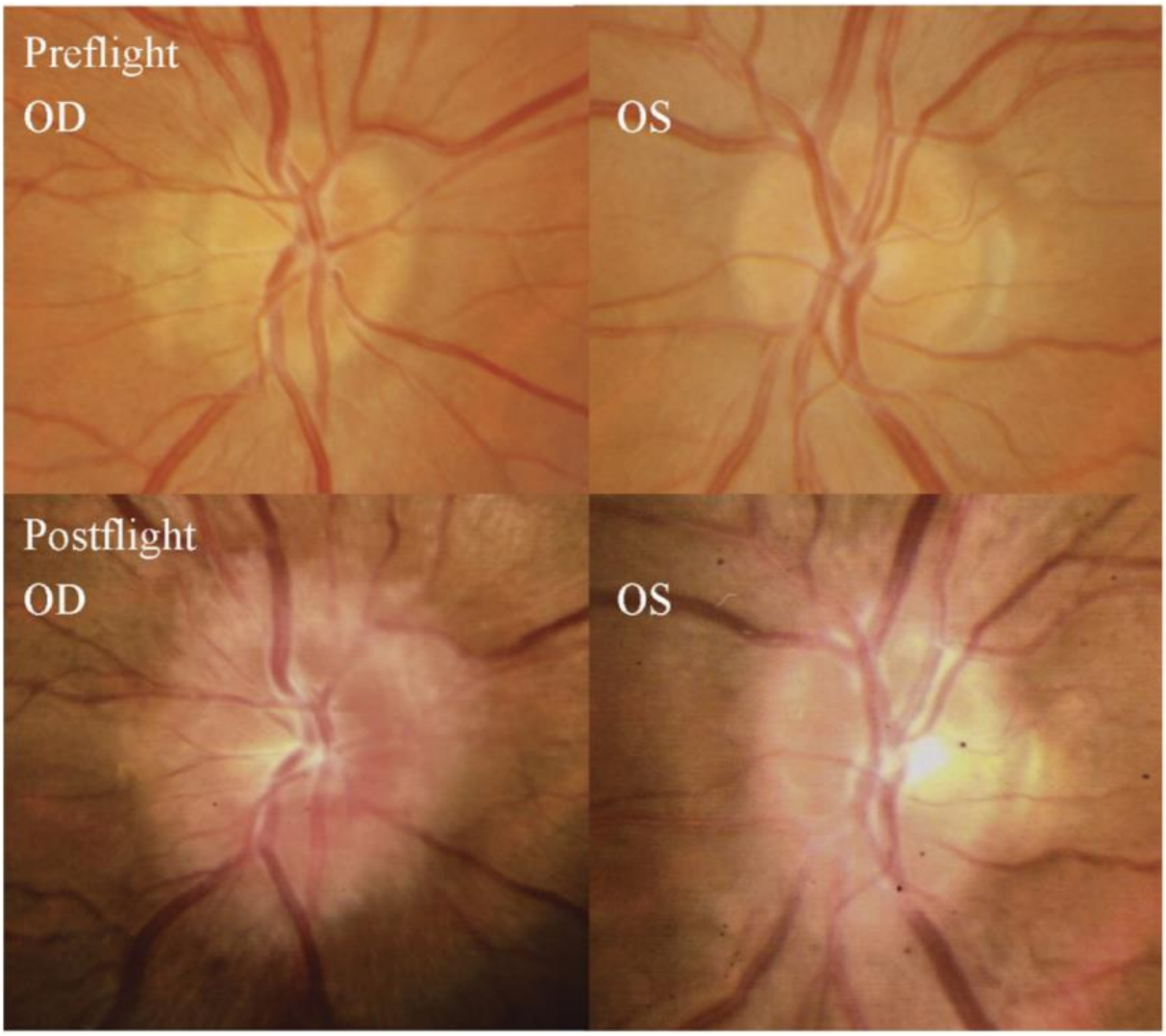

Figure 1.4. Pre- and post-flight fundus imaging of asymmetric optic disk edema in an astronaut. Oculus dexter (OD – right eye) and oculus sinister (OS – left eye) are both visualized (figure from 12).

Cotton Wool Spots

Described as fluffy white patches on the retina, cotton wool spots have been observed in some astronauts. They occur as a result of damage to nerve fibers due to the accumulation of axoplasmic material and is related to swelling of the retinal tissue. 3 out of 7 long-duration spaceflight astronauts, as well as the returning astronaut from the case study, developed cotton wool spot as a result of their missions according to Mader et al.[12,13]. SLO or DFE can be conducted to image the retina in order to observe cotton wool spots (Figure 1.5). Generally, these retinal abrasions tend to disappear after a number of weeks upon return but can persist for longer. Again, extended missions likely would increase the severity of their occurrence.

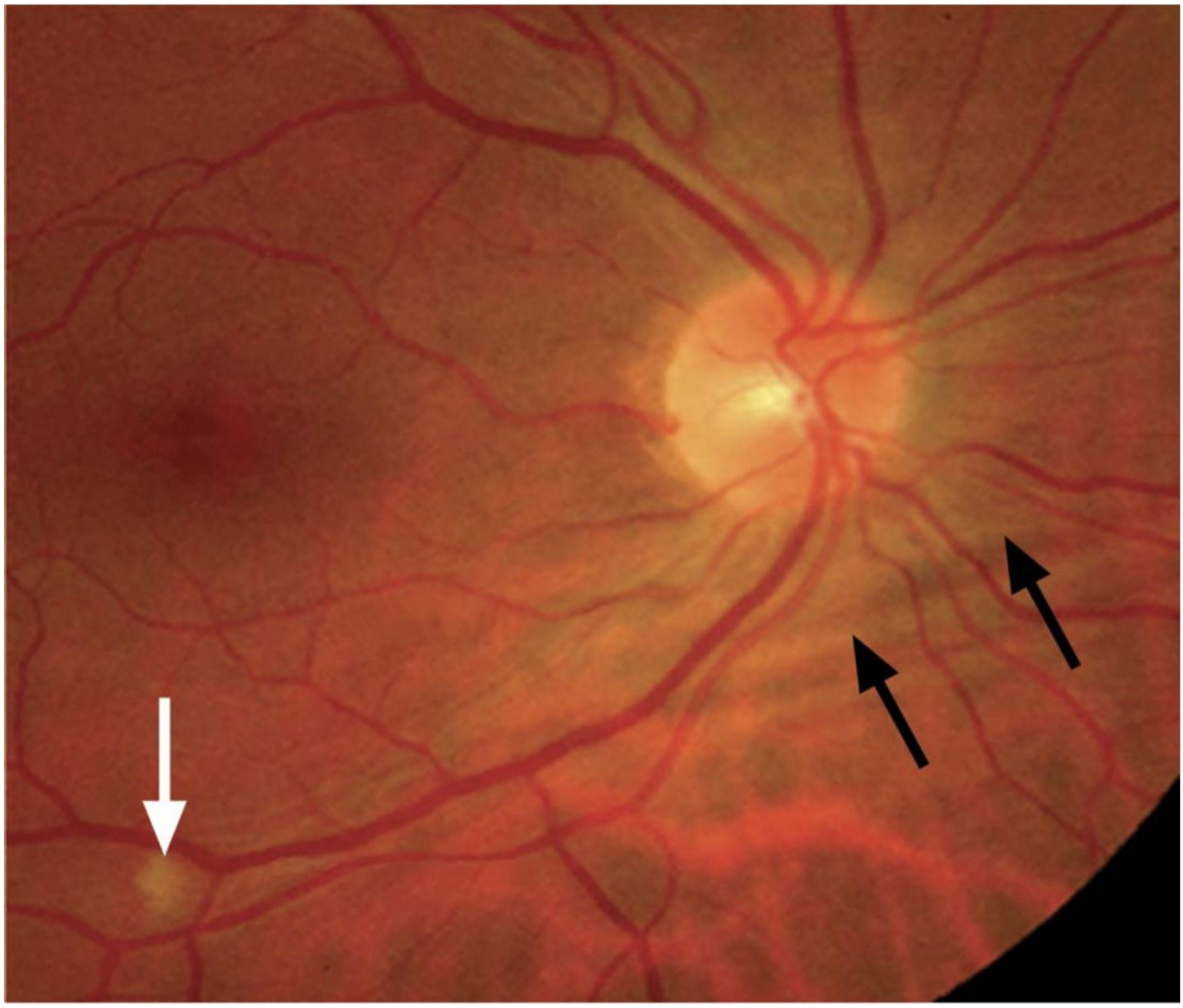

Figure 1.5. Fundus image of cotton wool spot (white arrow) observed in an astronaut after their first space mission. Choroidal folds (black arrows) are also highlighted (figure from 14).

Choroidal Folds

Another symptom associated with elevated pressure within the CSF around the posterior globe is the wrinkling of the choroid tissue layer termed choroidal folds. These folds can be often be visualized using SLO or DFE however spectral-domain optical coherence tomography (SD-OCT) has been frequently used to look at the individual fiber layers of the retina (figure 1.6). Mader et al. reported choroidal folds in 5 of 7 long-duration spaceflight

astronauts[12] and the reoccurrence of choroidal folds in one astronaut that returned to the ISS for a second mission[14].

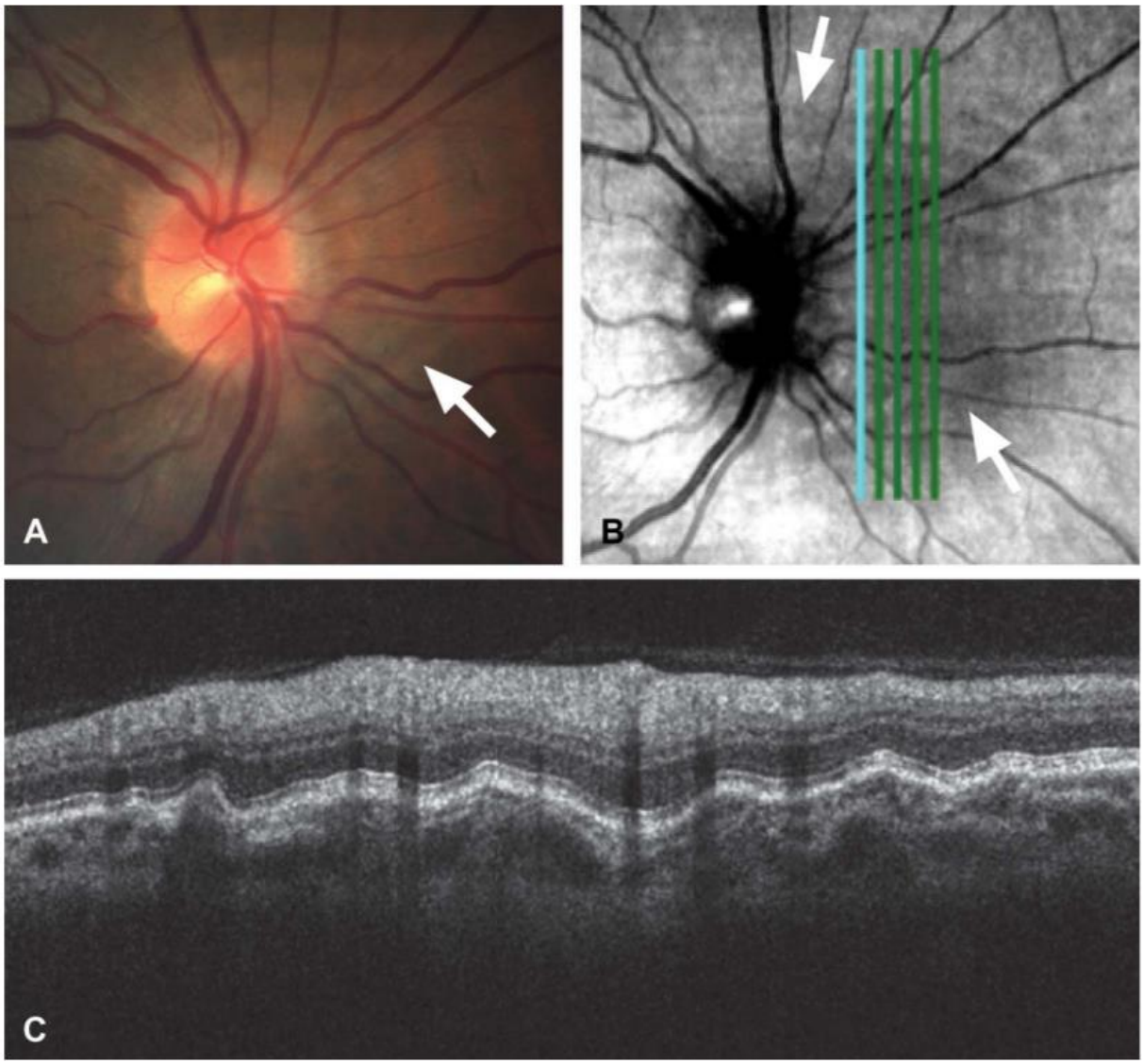

Figure 1.6. Choroidal folds overserved with various imaging techniques. Imaging types used to observe choroidal folds include a) dilated fundus examination, b) scanning laser ophthalmoscope, and c) spectral-domain optical coherence tomography. White arrows highlight location of choroidal folds (figure from 14).

Globe Flattening

Another SANS symptom observed in some long-duration spaceflight astronauts is the flattening of the posterior surface of the optic globe. High resolution MRI are commonly used

to observe these changes. Again, this occurrence is believed to result from elevated pressure within the CSF surrounding the ON but may also be due to the remodeling of tissues under microgravity conditions. Over time the pressure imbalance between CSF and intraocular pressure (IOP) is believed to allow for the shifting or compression of the retinal, choroidal, and scleral tissues (Figure 1.7 a, b). Ultimately this results in progressive degradation of vison, similar to hyperopia, causing concern for longer mission such as a trip to Mars. Interestingly, asymmetric globe flattening has been observed in the astronaut cohort[14] for which reasoning is still not well understood. This is in contradiction to terrestrial disorders such as idiopathic intracranial hypertension, in which both globes tend to be affected equally.

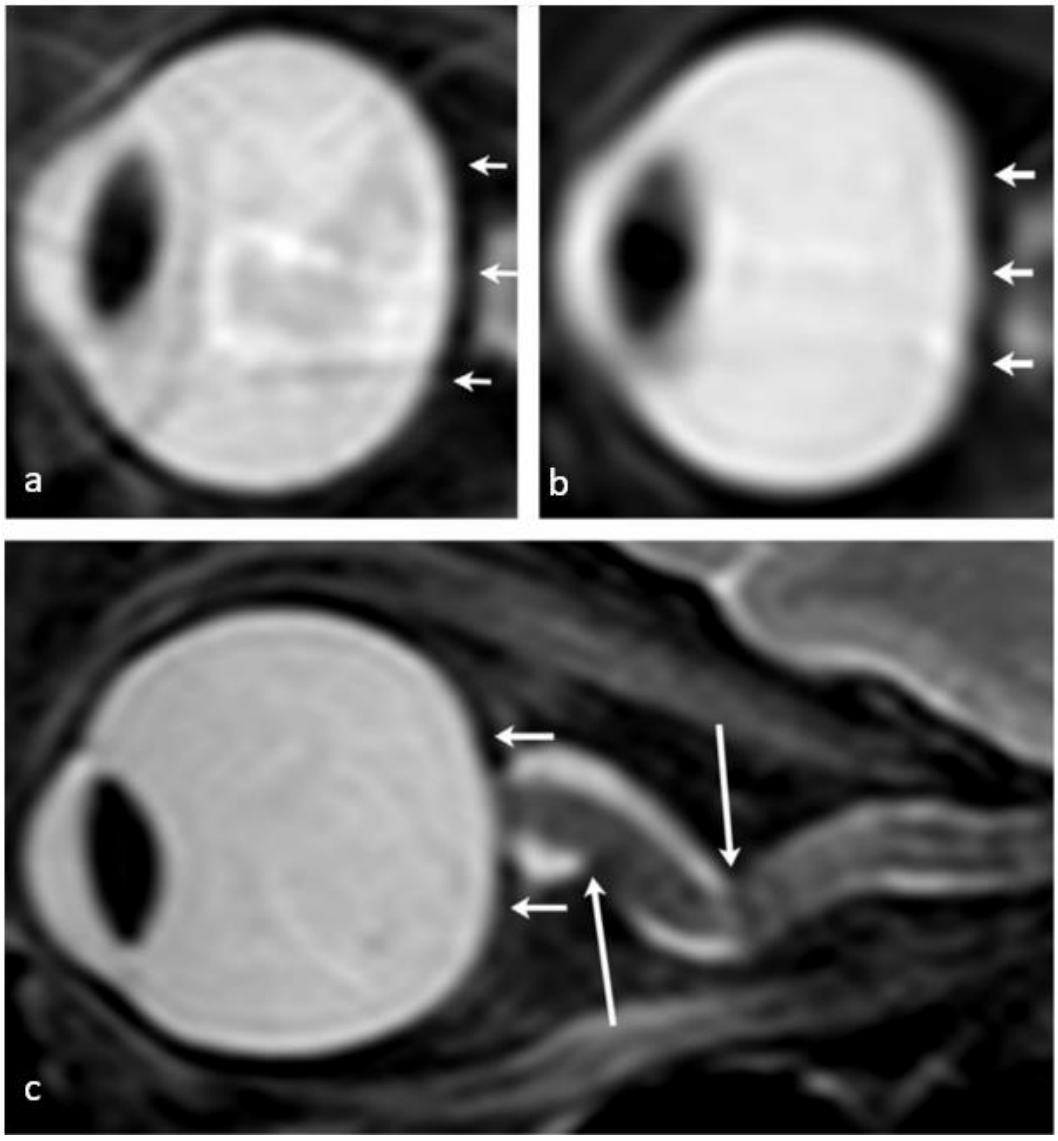

Figure 1.7. MR images highlighting globe flattening (short arrows) and nerve kinks (long arrows). An example pre-flight image (a) showing normal posterior globe surface and the associated post-flight image (b) for one astronaut. c) highlights a severe case of ON kinking in an astronaut after spaceflight (figure from 15).

Optic Nerve Tortuosity

In addition to these major symptoms, ON kinking has been observed in some long-duration spaceflight astronauts (Figure 1.7 c). This raises concern that the elevated ICP experienced by astronauts due to headward fluid shifts may be affecting the structure of the

ON as well. This could also potentially result in changes in vision and headaches that may ultimately be long term.

Possible countermeasures to combat SANS are difficult to produce since highly invasive procedures would be necessary to interface with ocular tissues. Additionally, we have no means to recreate gravity to avoid the occurrence of SANS symptoms while in space. Lower body negative pressure (LBNP) suits have been developed and are continually tested. These bulky suits are worn like a pant and mechanically create a negative pressure around the lower body in order to counteract the elevated pressure of the upper body. LBNP suits were shown to reduce ONS distension and CSF in the head in a study utilizing head-down tilt bed rest (Earth based microgravity analog)[16]. These suits show great promise for counteracting SANS like symptoms in long-duration spaceflight astronauts.

Ophthalmic Imaging Techniques

On Earth many different imaging techniques can be used for visualization of the various tissue structures of the eye. Ultrasound, SLO, DFE, and OCT can be used to image to structures around the posterior globe. Each of these techniques utilize the lens of the eye to access the tissues around the back of the eye. For tissues that are deeper within the cranium MRI techniques are used. Each of these techniques are described in detail.

Ultrasound

Ultrasound scans use high-frequency sound waves to visualize tissue structures. Sound waves can be sent into the body via a handheld transducer. These waves interact with tissues and depending on the density of the various tissues, echo back to the scanner or continue

through to the next tissue layers. The returning sound wave are recorded and transformed into an image which is then interpreted by a specialist. The advantages of ultrasound are that very minimal energy and equipment are required for imaging and there is no know adverse side effects to the body. Disadvantages include low resolution images and the need for extensive training to correctly operate and interpret the images.

Currently due to the minimal size and energy input required for ultrasound, this imaging technique is exclusively used on the ISS for monitoring ophthalmic changes. While this allows for useful measurements of some of the ocular structures, astronauts do not spend many years training to operate the equipment causing error in these measurements. Additionally, the resulting image produced from ultrasound is the lowest resolution and hardest to interpret of the imaging techniques discussed here.

Scanning Laser Ophthalmoscopy (SLO)

A monochromatic, low-powered laser light produced from a near-infrared diode is used to scan posterior surface of the optic globe and the ON head. This is performed in a raster fashion which is similar to how images are created on a monitor. This light is reflected by the tissue and collected by a photodiode and digitized as an image. A confocal filter is utilized to only collect light from location illuminated by the laser. This technique has been around since the 1980's and has allowed for high resolution imaging of the posterior globe. While still very useful DFE and OCT are more frequently used today.

Dilated Fundus Examination (DFE)

Fundus photography requires pupil dilation in order to increase the viewing window of the posterior globe for the camera to image. Essentially, fundus imaging is low powered microscope connected to a camera. Relatively simple in design and easy to operate. Color fundus imaging is often used today to observe the retina. Other than the discomfort of pupil dilation, fundus imaging is relatively non-invasive and painless.

Optical Coherence Tomography (OCT)

Optical coherence tomography is a modern-day high-resolution imaging technique that is used to produce three dimensional images of the various layers of the posterior eye in seconds. It is an optic analogue to ultrasound utilizing near-infrared light to determine reflectivity profile of tissues at the posterior surface of the eye. This technique is non-invasive, painless, and much quicker than other imaging techniques.

Magnetic Resonance Imaging (MRI)

Utilizing a large generated magnetic field, MRI can noninvasively create images of all the tissues within the body. When inside the coils of the machine our protons orient themselves in the direction of the powerful magnetic field. Carefully designed, well timed, radiofrequency pulses are utilized to adjust the orientation of these protons. As these protons realign with magnetic field, sensors in the MRI pick up the energy that is given off by their movement. Depending on the size and shape of the molecules they belong to this realignment

will occur at different times. Effectively, MRI is utilizing well timed radiofrequencies to image tissues based on chemical makeup.

Commonly, MRI are collected in two major types of weighting, T1- and T2-weighted MRI. These images vary in intensity between lipid rich and water rich tissues. For example, T1-weighted MRI depict fatty tissues such as axons of the brain in varying shades of white while water dense tissues like CSF appear dark. The opposite is true for T2-weighted images. This technology allows for the highest resolution imaging while also offering access to regions of the body, like the brain, that was not previously accessible. Unfortunately, for astronaut studies the large machinery and very high energy consumption required for this technology cannot be utilized in microgravity. Additionally, imaging sessions often require extended periods of time within the imaging coil. Higher resolution images, like the scans utilized in this study, take additional time to complete. This extended imaging time, in combination with the small space the subject must remain still within, can allow for movement artifacts and general discomfort.

Chapter 2: Research Objectives

The proposed research aimed to quantify alterations in ocular biomechanics due to space flight. Ocular biomechanics will be quantified based on non-invasive MRI measurements obtained for pre- and post-space flight astronauts (n=10, Figure 1). We will establish baseline values for ocular biomechanics in astronauts (Specific Aim 1), immediate post-flight values to observe altered ocular biomechanics resulting from spaceflight (Specific Aim 2), and to determine if these values recover to baseline over a one-year period (Specific Aim 3).

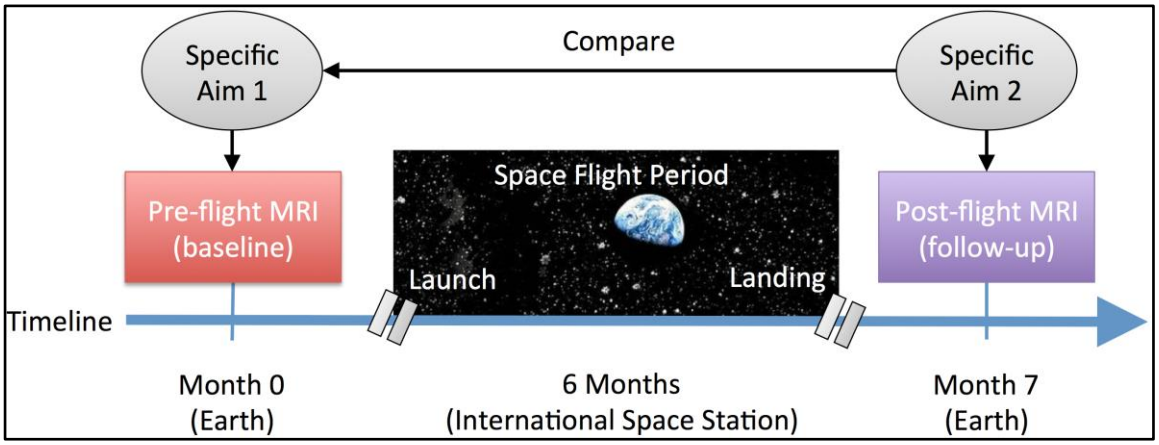

Figure 2.1. Overview of the proposed research study. MR images will be collected for astronauts (n=10) pre- and post- a 6-month space flight period. All images will be collected under an existing research grant within NASA Johnson Space Center. These images will be shared with University of Idaho for analysis of ocular biomechanics at baseline (Specific Aim 1) at immediate post-flight (Specific Aim 2) and for a one-year recovery period (Specific Aim 3).

Specific Aim 1

To quantify pre-flight ocular biomechanics in astronauts (n=10). This aim will allow us to understand the baseline variability in ocular biomechanics among an astronaut-like population.

Specific Aim 2

To quantify immediate post-flight ocular biomechanics in astronauts (n=10) and determine if measures of ocular biomechanics are altered due to space flight. This aim will allow us to test the hypothesis that space flight will result in a) increase in ON tortuosity, b) lack of change in ON geometry, c) distension of the ONS geometry, and d) increase in optic globe volumetric deformation (posterior globe flattening).

Specific Aim 3

To quantify recovery of ocular biomechanics in astronauts (n = 10) at five intervals over a one-year period after return from long-duration spaceflight missions.

Alignment with NASA and Idaho Space Grant Consortium Goals

The proposed research is in response to Idaho NASA EPSCoR Research Initiation Grant Program and aligns directly with NASA's Strategic Goals set forth in the Human Research Program *Risk of Spaceflight Associated Neuro-ocular Syndrome*, specifically to the following research Gaps SANS 1, 3, 12, and 13 (Table 2.1). In addition, the proposed research aligns the Idaho Space Grant Consortium (ISGC)'s Strategic Goals including science, technology, engineering and medicine (STEM) education that leads to new discoveries and a brighter future in Idaho.

Table 2.1. Aims of the proposed study

Aims of the proposed study	**HRP-47052 Rev. F Element**	**HRP-47052 Rev. F Risk**	**HRP-47052 Rev. F Gap**
1) Quantify alterations to ON Tortuosity as a result of long-duration spaceflight	Human Health and Countermeasures (HHC)	Risk of Spaceflight Associated Neuro-ocular Syndrome (SANS)	SANS3, SANS12
2) Quantify alterations to ON and ONS cross-sectional geometries as a result of long-duration spaceflight			SANS 13
3) Quantify posterior globe volumetric deformation as a result of long-duration spaceflight			SANS1, SANS12

SANS 1

We do not know the etiological mechanisms and contributing risk factors for ocular structural and functional changes seen in-flight and postflight.

SANS 3

We need a set of validated and minimally obtrusive diagnostic tools to measure and monitor changes in intracranial pressure, ocular structure, and ocular function.

SANS 12

We do not know whether ground-based analogs and/or models can simulate the spaceflight associated VIIP syndrome.

SANS 13

We need to identify preventative and treatment countermeasures (CMs) to mitigate changes in ocular structure and function and intracranial pressure during spaceflight.

Chapter 3: Magnetic Resonance Image Quantification of Changes to the Optic Nerve After Long-duration Spaceflight

Abstract

A subset of long-duration spaceflight astronauts have experienced ophthalmic abnormalities collectively termed SANS. Despite the urgency to counter SANS symptoms, little is understood about the pathophysiology of the syndrome. Microgravity induced elevated intracranial pressure (ICP), as a result of headward fluid shifts, is the major hypothesized reason for the occurrence of SANS. In particular, potential changes in ON tortuosity and ONS distension may have an underlying impact on ocular function. The present study aimed to provide a reliable, quantitative analysis of ON and ONS tortuosity and cross-sectional areas in long-duration spaceflight astronauts. High resolution MR images were collected both pre-flight and at five recovery timepoints post-flight for (n = 10) astronauts, extending to one year after return from 6-month duration international space station (ISS) missions. Manual and semi-automated methods were developed, reliability tested, and applied to assess ON tortuosity and ON/ONS cross-sectional areas for each subject. There were no significant spaceflight associated changes in all three parameters. The average and percent change in tortuosity, ON area, and ONS area immediately post-flight was -0.06 ± 0.42 mm (-0.9%), 0.58 ± 2.53 mm^2 (6.7%), and -0.88 ± 2.35 mm^2 (-3.7%) respectively. Parameter values at recovery time points were relatively consistent over time. However, a few outliers may indicate subject-specific spaceflight associated changes. Quantitative MRI based assessment of the ON and ONS could help our understanding of SANS and assist its prevention.

Introduction

Extended spaceflight is known to cause a number of physiological changes in humans including bone and muscular atrophy, vestibular dysfunction, and cardiovascular deconditioning[17]. As a result of extended space flight, some astronauts experience ophthalmic changes collectively labeled SANS[18]. Although the majority of astronauts did not develop visual impairment, SANS severity may increase with spaceflight duration and possibly result in permanent damage to the structure and function of the visual pathway. The pathology of SANS is denoted by decreased near visual acuity, globe flattening, optic disc edema, choroidal folds, retinal nerve fiber layer thickening, and cotton wool spots[12,15,19,20]. These changes may be impacted by ONS distension and ON tortuosity, clinically observed in astronauts by Mader et al. and Kramer et al[12,15]. Kramer et al. also measured the diameter of the mid-orbit ON and visible axonal section, which was significantly larger when kinks were present ($p = 0.1$)[15]. These descriptive findings are important but were semi-quantitative, with limited quantitative measures obtained in a two-dimensional plane. For example, ONS diameter was manually measured at a location 3 mm posterior to the ON head.

While the underlying mechanisms to explain SANS pathophysiology have not been unequivocally determined, the leading hypothesis is that a lack of a gravitational vector acting on the body results in a headward fluid shift and possibly mild, chronic elevation in ICP relative to the upright position on Earth. This headward fluid shift may shift additional cerebrospinal fluid (CSF) into the bulbar subarachnoid space surrounding the ON ultimately resulting in SANS in some individuals. In microgravity, it is hypothesized that the loss of the hydrostatic pressure gradient during spaceflight results in altered cephalad Starling-Landis fluid pressure factors

that may lead to elevated transcapillary filtration and tissue edema. It is also possible that a headward shift in CSF within the spinal subarachnoid space could decrease intracranial and ONS compliance. A loss in ONS compliance could exacerbate perineural forces at the back of the eye. Alterations to intracranial compliance have been implicated in several central nervous system pathologies such as normal pressure hydrocephalus.

The space medicine community have conducted numerous studies to help identify astronauts with SANS and possibly point to underlying etiological factors that lead to the condition. Several terrestrial pathologies have similar clinical signs and symptoms to astronauts with SANS. For example, tortuosity and distension of the ON and ONS is commonly reported in neurofibromatosis type 1 and idiopathic intracranial hypertension (IIH, also known as pseudotumor cerebri) patients. Neurofibromatosis type 1 patients also often display ON "kinking" [21,22] that shows some similarity to the descriptive ON kinking reported after long-duration spaceflight.[15] IIH, as an analogue to elevated ICP in space, can result in papilledema, perioptic subarachnoid space enlargement, and vision loss[23-25] similarly reported in SANS. Head-down-tilt (simulated microgravity fluid shift) bed rest studies have also assisted the investigation of SANS pathophysiology. Recent magnetic resonance imaging (MRI)-based findings by Roberts et al. possibly indicate that astronauts may have bulk displacement of various brain regions and alterations in CSF spaces following spaceflight[9]. These morphometric changes are similar to those observed in head-down-tilt bed rest studies.[26,27] Laurie et al. found that strict 6 degree head-down-tilt bed rest reproduced the optic disc edema and retinal nerve fiber layer thickening observed in long-duration spaceflight

astronauts.[28] In combination, these related pathologies and experimental techniques show potential to better understand SANS etiology.

Given NASA's goal for future exploration-class missions to other planetary bodies such as Mars, it is important that appropriate SANS countermeasures are developed. However, there remains a significant knowledge gap in quantification of ocular structural adaptions due to a) limited astronaut study population, b) 2D operator-dependent measurement methods, c) descriptive measurements often collected at a single time-point post-flight, d) lack of measurement reliability quantification. Quantifying potential changes occurring to the intraorbital ON and ONS may assist to fill some of these gaps. In this study, we developed semi-automated methods to quantify ON tortuosity and the subarachnoid space 3D geometry in long-duration spaceflight astronauts. A deeper understanding of how these adaptions relate to eye damage will potentially allow identification of risk factors and countermeasures to mitigate these adaptations.

Methods

MRI data collection for this study was approved by the NASA and University of Idaho institutional review boards and satisfied all local and international regulations for human subject research. All data was de-identified before data transfer to the University of Idaho for analysis.

Study Design

MRI scans were conducted on 10 astronauts from the Ocular Health study (NASA) on a 3T Siemens Verio scanner (Software ver. syngo MR B19, Munich, Germany). MRI scans that were collected pre-flight as a baseline were labeled as L-9/6 and L- 21/18. These labels stood for launch scan followed by the range in weeks prior to launch the scan was conducted. However, the actual time between the launch and scan times were significantly longer. Two of the ten astronauts completed both the L-21/18 and L-9/6 pre-flight scans while the remaining eight astronauts only completed the L-21/18 pre-flight scan. Being the closest scan to the launch date, the L-9/6 scan was used if it was conducted. If artifacts were found within the L-9/6 scan the L-21/18 scan was used. Five post-flight scans were also collected each to be used in comparison with the pre-flight launch scans. These scans were labeled R+1/3, R+30, R+90, R+180, and R +360. Labeling here stood for return and range of days the scan fell within after return from spaceflight. Nine of the ten astronauts completed the immediate post-flight R+1/3 scan. The immediate post-flight scan for the remaining astronaut fell into the R+30 category. Due to scan artifacts or lack of scan completion, some astronauts did not complete one or more of the five return scan windows. High resolution T1-weighted sagittal and T2-weighted coronal scans were collected to assess ON tortuosity as well as ON and ONS space cross-sectional areas, respectively. Parameters and reliability tests were generated for assessing changes in ocular structures.

Tortuosity Parameters

To quantify the degree of ON "kinking" (Figure 3.1), the following methods were applied to obtain tortuosity parameters for each astronaut pre- and post-flight. A volume of T1-weighted images was collected (Figure 2.1) with 900 µm slice thickness and spacing, 488 µm in-plane isotropic pixel size (FOV 512 x 512), repetition time TR=1900, echo time TE = 2.32, and 9° flip-angle. Curved ON trajectories were manually generated using the 3D curved multiplanar reconstruction tool within the OsirixMD dicom viewer (version 8.0.1, Pixmeo, Geneva, Switzerland).

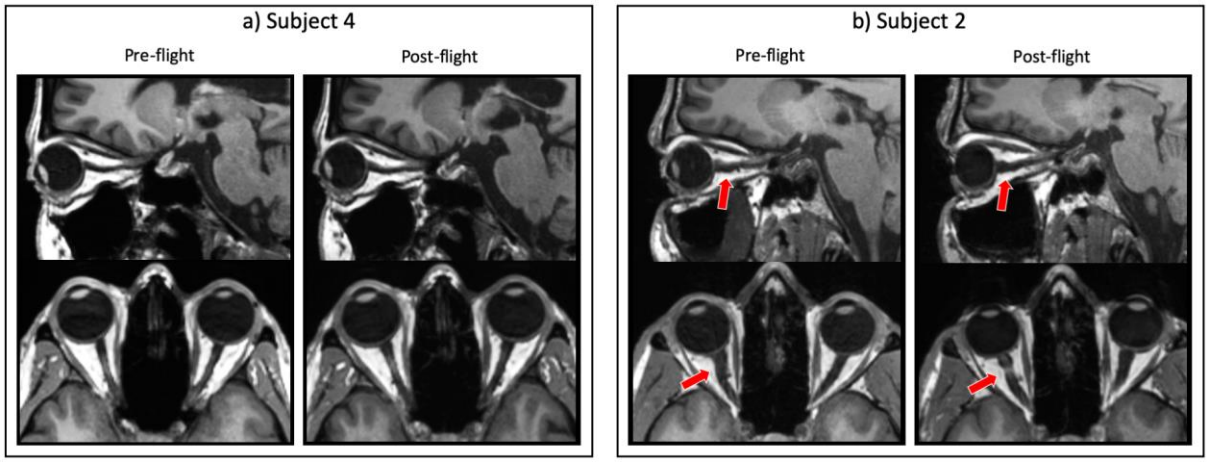

Figure 3.1. Sample MRI used for ON tortuosity quantification. Launch (pre-flight) and R+1/3 (post-flight) T1-weighted sagittal MRI of two astronauts showing ON a) without and b) with tortuosity after spaceflight. Arrows highlight ON kink location.

The X, Y, Z-coordinates for points along the trajectory were selected at the ON centerline with ~1-2 mm spacing and exported as comma separated values (Figure 3.2a, 3.2c). An up sampled spline curve was fit to the points and truncated at a length of 20 mm using MATLAB (Ver. 2015a, Mathworks, Natick, MA). A curved trajectory length of 20 mm was used because this length covered the region of ON kinking that was present in some astronauts. The X, Y, Z-coordinate of the lens center and ON head was selected based on multi-planar

visual inspection. Tortuosity was determined based on the maximum orthogonal distance between the curved ON trajectory and a straight line connecting the ON head and a point on the ON trajectory located 20 mm posterior to the ON head (Figure 3.2b).

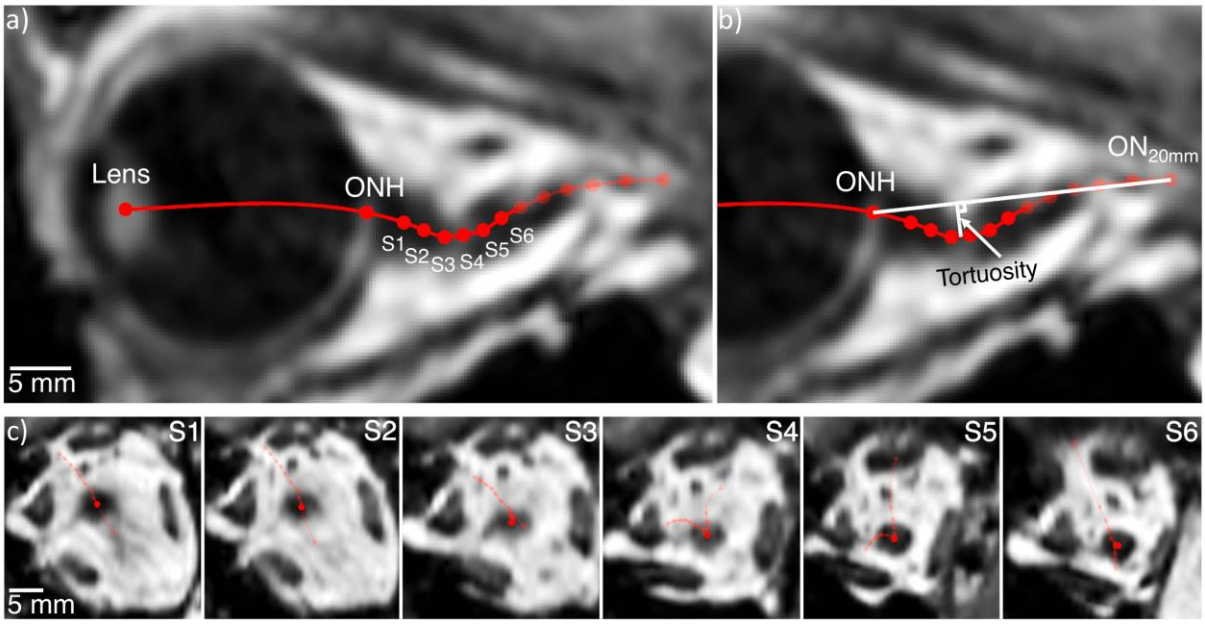

Figure 3.2. ON pathways were selected manually (for example, S1, …, S6) starting with lens center and ON head location. a) Visualization of ON pathway selections (red). b) Visualization of the tortuosity length (white arrow) measured as the distance between interpolated points along the ON trajectory (red) and the corresponding Euclidean line from ON head to final point along ON pathway (white). c) 3D multi-planar reconstruction showing coronal view of each selection (S1-S6) along the same ON trajectory centerline (red) shown in a).

ON and ONS Geometric Parameters

To assess ONS distension, 3D geometries of the ON and ONS were quantified using the following semi-automated method. High-resolution T2-weighted coronal MRI scans were collected (Figure 3.3a) with 600 µm slice thickness and spacing, 253 µm in-plane isotropic pixel size (FOV 256 x 256), repetition time TR = 820, echo time TE = 118, and 170° flip-angle. We applied a global thresholding method to extract ON and ONS contours. This process was selected due to consistent FOV illumination and the bimodal nature of the intensity distribution[29]. Global thresholding algorithms utilize the bimodal nature of the histogram

representing an image's intensity profile to isolate an object. In this case the object was the boundaries of the CSF space which define the ON and ONS cross-sectional areas in a given slice of the MRI. For the MRI sequence used the higher intensities represented water dense tissues while the remaining tissues represented the lower intensity values. Together these tissue types made up the observed bimodal nature of the image's intensity histogram.

Between scans we observed variability in overall scan brightness which would lead to contouring errors if the same threshold was used for each scan. This is a result of an increase in peak intensity associated with larger volumes of CSF. With varying volumes of CSF the associated signal collected by the MRI changes proportionally. This raised concern that reliability of threshold-based contouring of the CSF boundaries may be affected pre- to post-flight where elevated CSF volume has been observed to increase. Thus, we adapted a threshold value using the following process. First, average background pixel intensity for each scan was computed, with the intensity ranging from 0 to 4095 (12-bit image), excluding the influence of potential volumetric changes in CSF. The background was selected with a slice-by-slice mask relative to the peak frequency (representing the water dense CSF space) in the pixel intensity histogram. By excluding these frequencies, the background tissues could be analyzed without out the influence of the CSF. There was no trend in background tissue pixel intensity change (-1.141 ± 5.708, average ± standard deviation) for subjects pre- to post-flight. A threshold was then chosen by adding the difference between the average intensity across all scans and the current scan to a common value. MRI slices were cubically up sampled and contoured in MATLAB with the computed threshold (Figure 3.3b). ON and ONS contours were automatically selected using a point count filter and isoperimetric difference quotient

(roundness measure). The ON head coordinate was manually selected for each case based on multiplanar reconstruction. Linear interpolation between contours (600 μm slice spacing) was applied to obtain a single contour located 3 mm posterior to the ON head along the nerve trajectory. Contours at varying distances from the ON head could also be generated providing a 3D representation of the ON and ONS (Figure 3.3c). ON and ONS cross-sectional areas 3 mm posterior to the ON head were then computed.

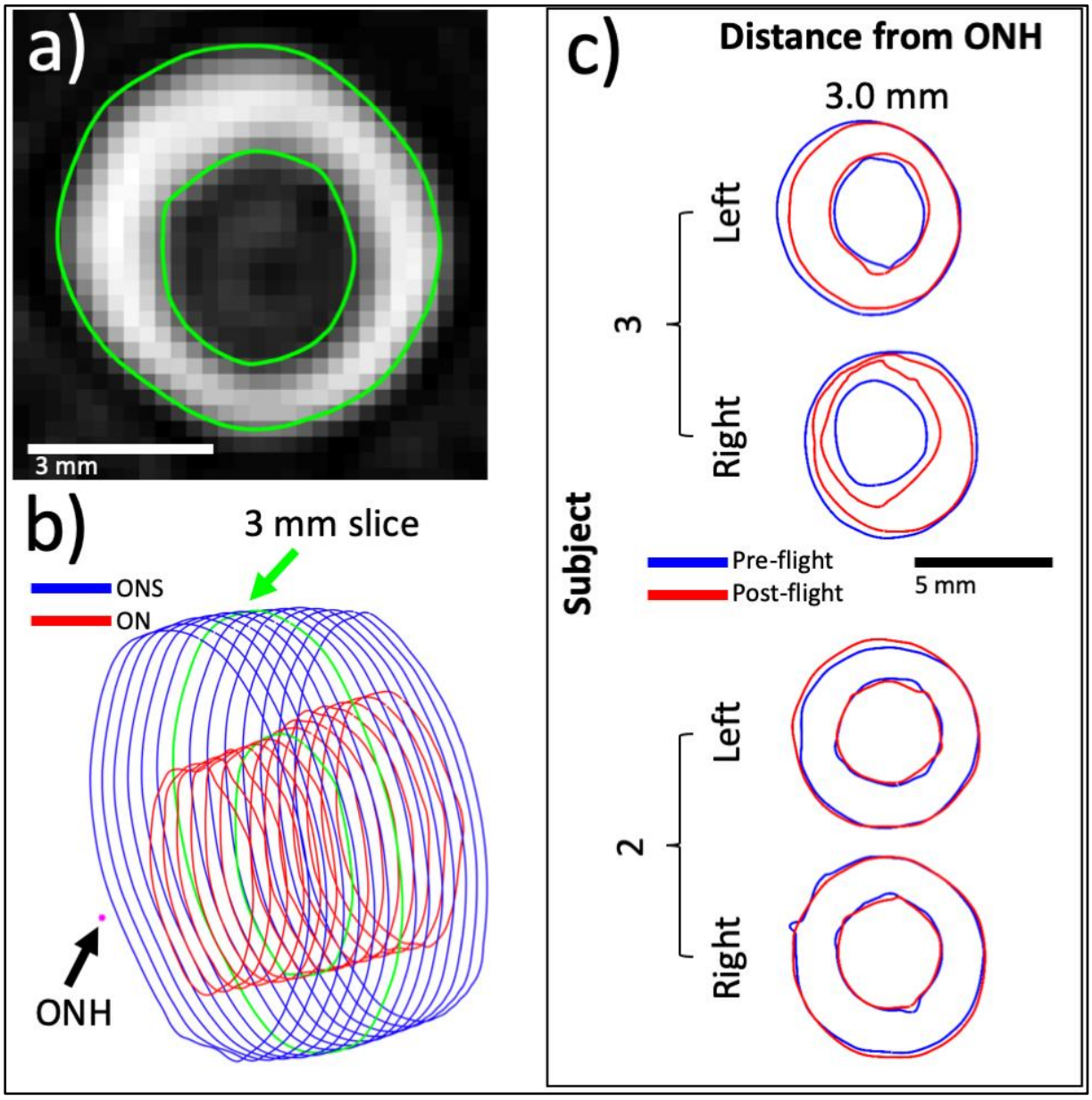

Figure 3.3. a) Example contour generation of the ON and ONS boundaries for a slice at 3 mm posterior to the ON head. b) Combined ON (red) and ONS (blue) contours for multiple slices including 3 mm slice contours (green), and c) an example of pre- versus post-flight contours for two subjects showing largest ON increase (top) and largest ONS increase (bottom) at 3 mm slice.

Reliability Assessment

Tortuosity parameter inter-operator reliability was quantified based on four trained expert operators. Each operator manually measured all parameters on three representative MRI data sets on a single day. Each operator repeated these measurements on three separate

occasions separated by at least a three-day interval. This was done to reduce possible influence of memory on trajectory point selections. Intra-operator reliability was quantified based on measurements performed by a single operator conducted on five days separated by at least a three-day interval for the same three MRI data sets. The average value for each tortuosity parameter was computed for the inter- and intra-operator reliability studies. The reliability of the tortuosity measurement parameter was computed as the mean difference of the individual cases from the average value and the standard deviation of the mean differences. Because there is no gold standard for this measurement, the mean value of all reliability measurement was assumed to be the true value.

ON and ONS cross-sectional area reliability was quantified by conducting an MRI phantom study. Phantom studies are conducted to analyze imaging performance by scanning an object of know dimensions. A phantom model was designed to contain three repeated idealized optic subarachnoid space geometries and three subject-specific geometries with a 2 cm axial length (Figure 3.4). Idealized geometries were represented by an ONS diameter starting from 7 mm and tapering to 5 mm. A concentric ON was placed in the center of the ONS with a diameter of 3.35 mm. The subject-specific geometry was created based on a segmentation of a representative astronaut optic subarachnoid space produced by the above methods. The phantom model was printed in WaterShed XC material (Koninklijke DSM N.V., Heerlen, Netherlands) by high-resolution SLA printing technology with a 50 µm layer thickness and 15 µm in-plane resolution. To our knowledge this is the first time a high-resolution 3D printed model of the ON and ONS has been constructed. The phantom was scanned twice on the same 3T MRI machine used for astronauts in this study. MRI images were processed using

an identical procedure used to assess the ON and ONS cross-sectional area in the astronauts. The mean and standard deviation of the difference in computed area from the known phantom model area (prescribed by the printer) was determined for the idealized and subject-specific model cases.

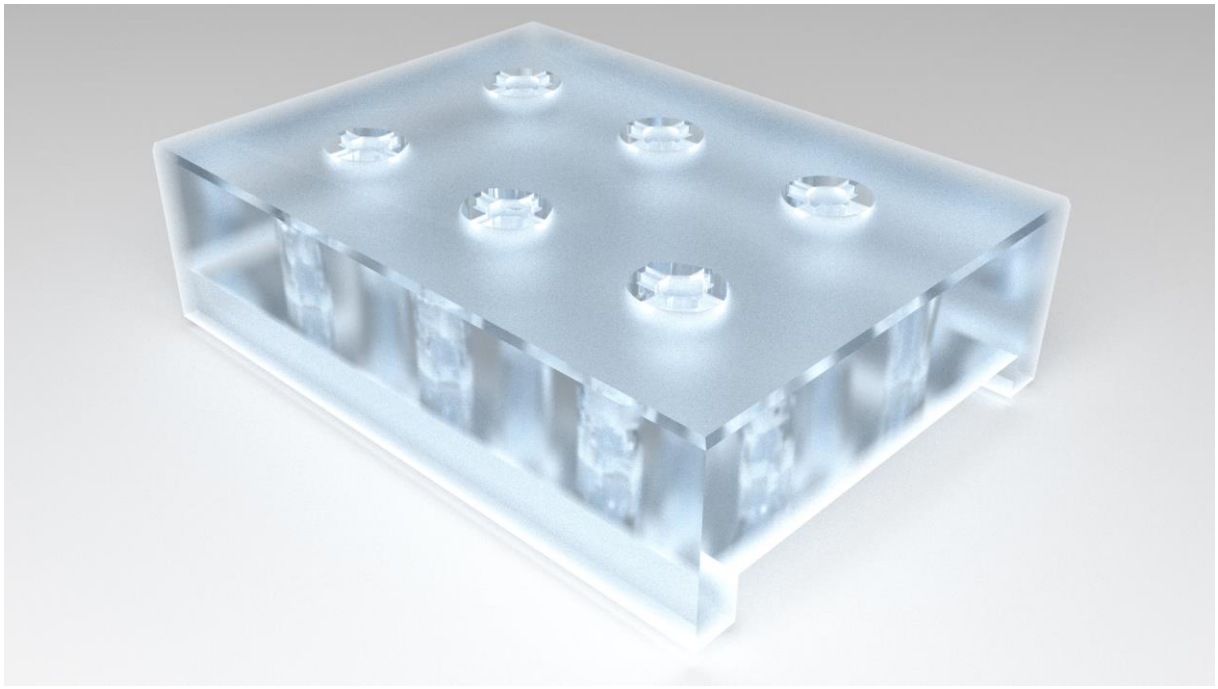

Figure 3.4. Phantom model including three of both idealized and subject specific ON and ONS geometries

Statistics

Descriptive statistics were performed to obtain the mean and standard deviation of the change in each parameter (post-fight minus pre-flight). Limited subject numbers did not allow analysis by sex.

Results

Non-invasive MRI data was collected for a total of 10 astronauts (average height, weight, and flight duration with standard deviation: 1.8 ± 0.1 m, 76 ± 9 kg, and 167 ± 17 days) at launch (508 ± 230 days pre-launch) and five recovery time-points after return: R+1/3 (4 ± 2 days), R+30 (31 ± 5 days), R+90 (101 ± 16 days), R+180 (188 ± 15), and 360 days (355 ± 14 days). Average spaceflight mission duration was 167 ± 17 days. A summary of all parameter results and reliability assessment is shown in Table 3.1.

Table 2.1. Average change and estimated reliability for each parameter. Reliability values correspond to the associated intra- and inter-reliability and phantom model assessment for tortuosity and ON/ONS variables respectively.

Parameter	Average Change ± Standard Deviation	Estimated Parameter Reliability
ON Tortuosity (mm)	-0.06 ± 0.42 (-0.9%)	0.15 ± 0.11 (intra-operator) 0.13 ± 0.11 (inter-operator)
ON Cross-sectional Area (mm^2)	0.58 ± 2.53 (6.7%)	0.36 ± 0.24 (idealized phantom) 0.23 ± 0.19 (subject-specific phantom)
ONS Cross-sectional Area (mm^2)	-0.88 ± 2.35 (-3.1%)	0.50 ± 0.41 (idealized phantom) 0.65 ± 0.73 (subject-specific phantom)

Optic Nerve Tortuosity

ON tortuosity was assessed in 8 of the 10 astronauts pre- and post-flight. MR image artifacts were present in two data sets and did not allow for tortuosity assessment. Of the 8 astronauts analyzed (n = 16 eyes), average change in ON tortuosity did not change pre- to post-flight (-0.06 ± 0.42 mm) (Table 3.1). Tortuosity remained unchanged through all timepoints (Figure 3.5 a). There were a few sizeable increases in tortuosity between the first two post-flight timepoints (R+1/3, R+30). Tortuosity (Figure 3.5 b) showed a strong linear

correlation between pre- versus immediate post-flight (R+1/3) values (R^2 = 0.72). This correlation was closely matched pre- versus post-flight, indicating a lack of change in ON tortuosity across the study population. Tortuosity for subject 9 (both nerves) notably decreased relative to the overall sample (Figure 3.5 b).

ON and ONS Cross-Sectional Area

ON and ONS cross-sectional areas were analyzed in 5 of the 10 astronauts (n = 9 eyes) due to MRI image artifacts or missing data (pre- or post-flight high-resolution T2-weighted coronal MRI data not collected). Average change in ON area from pre- to immediate post-flight was 0.58 ± 2.53 mm^2 (Table 3.1). The ON area values (Figure 3.5 c) tended to decrease pre- to initial post-flight excluding a large increase for one subject. ON areas showed a weak linear correlation (Figure 3.5 d) between pre- and post-flight values (R^2 = 0.13). Contours for the subject with the largest ON area increase (3R) were visualized in Figure 3.3 c.

For the five astronauts analyzed (n = 9 eyes), pre- to immediately post-flight ONS average change and standard deviation was -0.88 ± 2.35 mm^2. The ONS cross-sectional area values (Figure 3.5 e) were fairly consistent across all time points for each subject. ONS cross-sectional areas showed a strong linear correlation (Figure 3.5 f) between pre- and post-flight measurements (R^2 = 0.91).

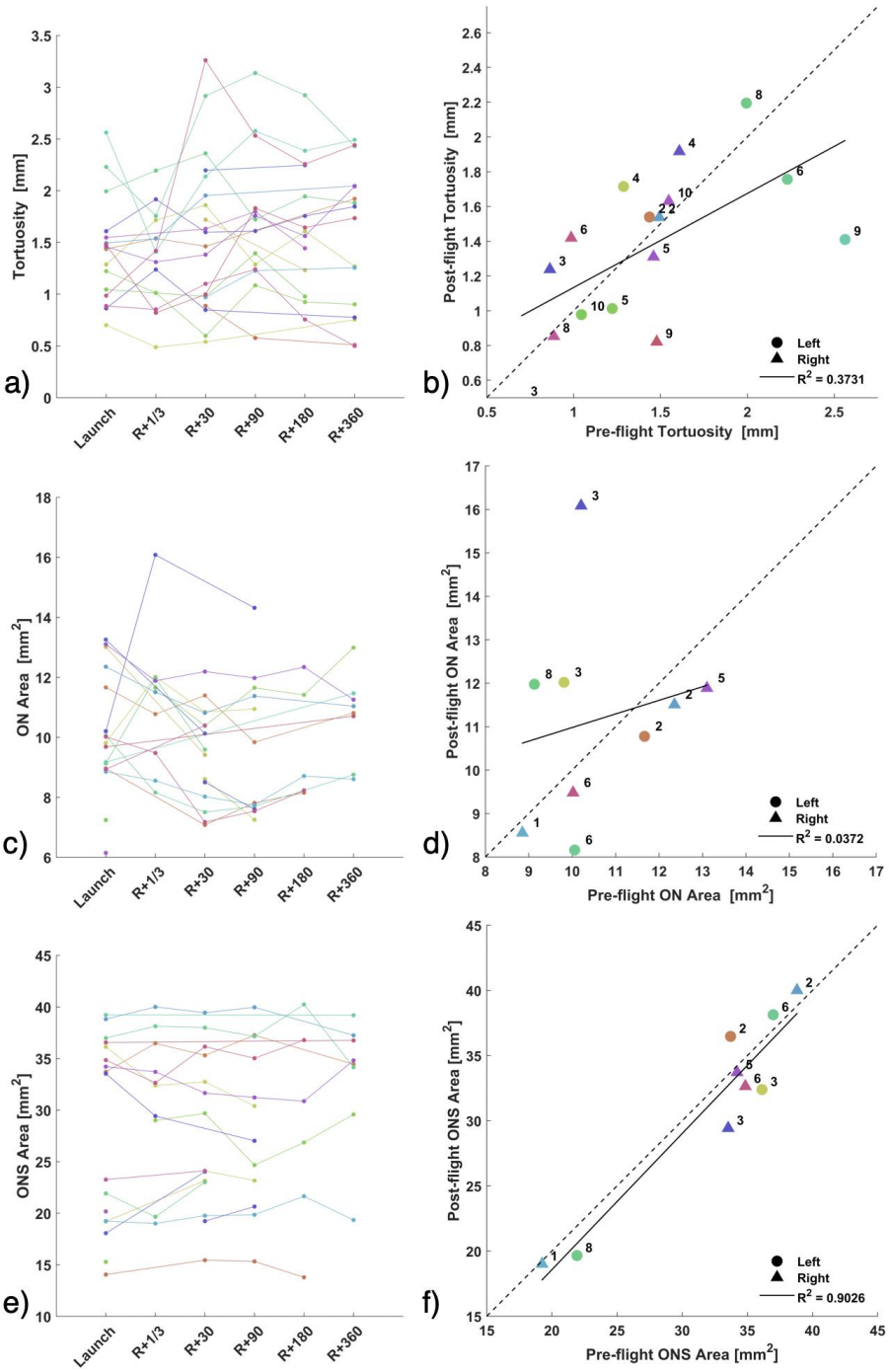

Figure 3.5. a) Time series showing tortuosity values measured at launch, R+1/3, R+30, R+90, R+180, and R+360. b) Correlation plot for launch versus R+1/3 tortuosity with linear correlation coefficient (R^2). Change in ON and ONS cross-sectional area pre- versus post-flight lacked a trend for the astronauts analyzed. c) Time series showing ON cross-sectional area 3 mm posterior to the ON head measured at launch, R+1/3, R+30, R+90, R+180, and R+360. d) Correlation plot for launch versus R+1/3 ON cross-sectional area 3 mm posterior to the ON head with linear correlation coefficient (R^2), e) Time series showing ONS cross-sectional area measured at launch, R+1/3, R+30, R+90, R+180, and R+360, and f) Correlation plot for launch versus R+1/3 ONS cross-sectional area with linear correlation coefficient (R^2). Note: Triangles represent the right eye, and circles represent the left eye. Line colors represent individual eyes and correspond across left and right plots in same row. Subject numbers are given for each astronaut and consistent across plots.

Reliability Assessment

Intra- and inter-operator reliability for tortuosity was 151.7 ± 111.6 and 131.6 ± 113.7 μm, respectively (11.9 ± 8.8 and 9.9 ± 8.5%). Phantom model ON and ONS reliability was 0.361 ± 0.239 and 0.496 ± 0.412 mm^2 respectively for the idealized geometries (1.69 ± 1.06 and 0.86 ± 0.66%). ON and ONS reliability was 0.231 ± 0.188 and 0.652 ± 0.727 mm^2, respectively for subject-specific geometries (1.86 ± 1.41 and 0.95 ± 0.65%).

Discussion

Comparison to Previous Studies

ONS Distension

Automated quantification of the intraorbital subarachnoid space revealed a lack of statistically significant changes to the ONS for the limited population of long-duration spaceflight astronauts analyzed. Additionally, recovery scans, collected the following year after spaceflight, showed consistency in ONS area measurements. These findings suggest that intraorbital CSF pressure may not be pathologically elevated in astronauts following exposure to microgravity since the ONS is known to be sensitive to pressure changes[30,31]. We also found that inter-subject differences in ONS area were much larger than intra-subject differences across time points. This shows that individual ONS cross-sectional areas are notably different and these differences persisted throughout the study, a potential indication of method reliability alongside the phantom model study. Kramer et al. observed a positive relationship between the degree of ONS kinking and ONS diameter. For the limited number of astronauts analyzed in our study, the degree of kinking measured by our tortuosity parameter lacked

correlation with ONS cross-sectional area (R^2 = 0.22). As described by Kramer et. al. the trabeculae, pillars, and septa of the subarachnoid space in a region of ONS kinking could compress and compartmentalize CSF pressure along the ON axis[15]. This could ultimately lead to the distension of the bulbar region of the ONS that has previously been observed in other astronaut studies[12-15,32]. Since ONS and increased kinking of the ONS was not observed in the present study, we do not speculate compartmentalization of CSF pressure.

Previous studies have conflicting results for spaceflight associated changes to the ONS. In combination, these study findings were limited to relatively small sample sizes and lacked paired tests conducted over multiple time points. Mader et al. reported ONS distension with MRI in multiple astronaut studies[12-14]. In these studies, however, ONS distension was either simply observed rather than quantified or the sample size was very low. One case report noted a maximum ONS diameter increase of 0.2 mm pre-flight to post-flight[14]. Ultrasound has been used to measure ON and ONS diameter in astronauts during flight as well. In one study, 13 of 14 long-duration astronauts were scanned with ultrasound at various stages of before, during, and after their mission. An average ONS diameter increase of 0.91 mm reported from pre- to post-flight, roughly an 11% change ($p = 0.012$)[32]. Unfortunately, this study reported average results obtained from different astronauts without sample paring across time points. The observed differences may have stemmed from inter-subject ONS variations rather than due to spaceflight. In a study by Kramer et. al., ON and ONS diameters were measured in 27 astronauts (8 of which completed a second mission allowing for control data). For the 8 astronauts with control scans, there was no significant difference in ONS diameter measured at a location 4 mm posterior to the globe (6.65 ± 1.42 to 6.66 ± 1.72 mm, $p = 0.97$). For our

study, ONS cross-sectional areas were quantified in 2D based on an automated segmentation algorithm. Although these cross-sections were not perfectly circular, if we assume a circular cross-section, our study ONS diameters have comparable values to Kramer et al. with values of 6.36 ± 0.73 mm pre-flight and 6.27 ± 0.80 mm post-flight. Interestingly, Kramer et al. found that 4 of the 27 astronauts analyzed showed significantly increased ONS diameters relative to an ONS kink with ONS diameter measurements of 7.5 mm ± 1.1 ($p = 0.03$)[15]. We observed little change in ONS tortuosity for any of the astronauts pre- versus post-flight (Figure 3.5 e, f).

ON Cross-Sectional Area

On average, ON area tended to decrease in this population of astronauts at R+1/3 (Figure 3.5 c, d), albeit these changes were near the measurement reliability. To our knowledge, no other MRI-based study has measured changes in the ON pre- to post-flight in a long-duration spaceflight astronaut cohort. Thus, we are not able to compare our ON results to previous work. Inter-subject differences were greater than intra-subject, and these differences persisted across recovery time points indicating potential consistency of the automated ON segmentation method. One outlier showed a large increase in ON area. Interestingly, this same subject had the largest decrease in ONS area. Additionally, the three subjects with an increase in ON area had a concomitant decrease in ONS area. This may indicate a reduction in bulbar subarachnoid space CSF pressure leading to deflation of the ONS and expansion of the ON. However, a decrease in CSF pressure would not be intuitively expected for a headward fluid sift of CSF.

Tortuosity

The astronauts in our study lacked a significant change in tortuosity over spaceflight (Figure 3.5 a, b). Similar to ONS and ON areas, the inter-subject differences tended to be larger than intra-subject differences, potentially indicating reliability of the method. Our method quantified tortuosity as the maximum orthogonal distance from the curved ON path to a straight-line path connecting a point 20 mm along the ON to the ON head. We chose to measure the maximum orthogonal distance as it gives a more intuitive measure of how much the ON deviates in terms of a linear measurement. Previous researchers quantified ON tortuosity as a ratio of ON curved path length to the Euclidean length in healthy adults as well as patients with glaucoma[33]. For 10 healthy Chinese adults, this ratio was on average 1.013 ± 0.019 for a standard forward gaze. When the eye underwent abduction, causing the ON to move notably, a peak ratio of 1.033 ± 0.034 was observed. For comparison, we computed this ratio-based measurement for the astronaut population and found average pre- and post-flight tortuosity ratio was 1.019 ± 0.013 to 1.017 ± 0.008, respectively. This value indicates that the astronaut population had a similar degree of tortuosity as healthy Chinese adults.

ON tortuosity has been reported in previous astronaut studies[14,15]. A drawback of these studies is that the change in tortuosity was not measured pre- to post-flight. Thus, it is not clear if ON tortuosity developed during flight, or if it was already present at baseline. We sought to apply a robust method using multiplanar reconstruction visualization to select the ON centerline. In addition, we conducted an inter- and inter-operator reliability study to help understand what the bounds of ON reliability. Although there were changes in tortuosity greater than the reliability bounds, the observed changes were relatively small on average. We were aware that the astronauts gaze may impact tortuosity measurement. Thus,

astronauts were instructed to fixate on a target straight ahead in the scanner. Based on visual inspection of the MRI scans, no significant abduction occurred in any of the astronauts analyzed.

Data Acquisition Techniques

Measurements for the ON and ONS have been obtained using multiple imaging techniques. Often ultrasound is used for real-time measurements both on Earth and on board the ISS. Computer tomography and MRI have been frequently used as well, allowing for visualization of 3D structures and varying tissue types. one advantage of the high-resolution MRI used for the present study is that it allows multiplanar imaging for many cross-sections of the ON at locations relatively deep with respect to the ON head. Unfortunately, MRI has a drawback in that it cannot, at present, be obtained in flight. Thus, we can only speculate how changes seen post-flight relate to in-flight status. Ultrasound is currently our best imaging option during spaceflight but offers a reduced quality of data and can produce error if the operator orients the transducer incorrectly along the ON axis midline. In general, previous studies have measured the ON and ONS diameters assuming a circular-shaped cross section. To further improve these measurements, we developed an automated contouring technique to calculate 2D ON and ONS cross sectional area change at a position precisely 3 mm posterior to the ON head. Our phantom model study showed <2% error in cross sectional area calculations, adding confidence to our results. Utilizing these techniques in future analyses

may offer more information about the distribution of pressure through the ocular CSF space in astronauts or under head-down-tilt bed rest.

Relevance to SANS

A single subject in our study (subject 2, Figures 3.1 b, 3.3 c, 3.5 e, f) was clinically diagnosed with Fundus grade edema call (SANS). This subject did not have a notable increase in ONS area. However, this subject did have the largest pe- and post-flight observed ONS area (Figure 3.5 f, right eye). Interestingly, Kramer et al. found a geometrically larger ONS in subjects with globe flattening, another symptom of SANS[15]. Subject 2 did not exhibit kinks to the ON or ONS and maintained some of the smallest values observed for tortuosity in this study. Unfortunately, subject 2 was the only astronaut in our population with SANS. Thus, it is not possible to deduce a trend for astronauts with SANS versus without.

Numerous studies investigating SANS analogues report ONS distension as a direct consequence of elevated ICP. While there is physiological dissimilarity between IIH and SANS related ICP changes, causal comparison can still be made between the two. It has been suggested that ONS diameter can be used to diagnose IIH[34]. Head-down tilt studies have been conducted in many human and non-human studies showing a demonstrative effect of intraocular pressure increases on the ONS. These results are a convincing analogue for pressure related changes in a microgravity environment. In the present study, we did not observe a trend in ONS cross-sectional area increase. This may indicate that the ON subarachnoid space is not sensitive to microgravity induced ICP elevation due to low ONS

compliance or the that ICP is not significantly elevated in space. Alternatively, it may indicate that the ONS area decreased immediately following return to Earth and that any changes during flight quickly returned to normal. Our average time for R+1/3 MRI scan was 4 ± 2 days. Unfortunately, the protocol did not allow decreasing this time point any earlier post-return.

It has been hypothesized that compartmentalization of the intraorbital subarachnoid space leads to inadequate redistribution of CSF. In particular, with the loss of gravity assisted transport, accumulated CSF in the perineural subarachnoid space could become trapped potentially damaging axonal structure of the ON[35]. In the current study, the lack of lasting changes in cross-sectional area suggest that compartmentalization does not play a significant role. While it is known that ONS changes to a varying degree with changes in ICP, known microgravity related ICP changes do not appear to have a remodeling effect on the visible structure of the ON/ONS. However, compartmentalization may be a factor in subjects with ON kinking which was also not observed in our astronaut population.

Limitations

It is important to note that for the contouring process, pixel intensities were globally shifted rather than normalized in order to maintain neighboring voxel intensity relationships. This is important because the fluid-tissue intensity interface is used to define measured contours. Therefore, the original voxel to voxel relationship must be maintained. We decided to maintain this relationship in order to take a conservative approach with our analysis. It has been noted that histogram mapping techniques have frequently been used to compare MRIs,

however these studies suffer from a lack of biological interpretability of the normalized units.[36] In this study, background tissue intensities of the fatty tissues surrounding the ON and ONS were used to define the offset values on a scan to scan basis. These tissues are observed to remain unchanged as a result of extended spaceflight and allow for the intensity offsetting necessary to compare appropriate fluid-tissue interfaces both among intra- and inter-subject scans.

Manual selection of the ON head as a zero point for the purpose of interpolating the 3 mm cross-sectional are contours inherently introduces error into the measure. However, we considered this error to be acceptable since MRI and point cloud registration would be limited by the FOV of the scan and movement of the ON. This decision was also impacted by intra-subject variability in the number of assessable slices.

Tortuosity assessment utilized T1-weighted MRIs rather than T2-weighted. Though the ON and ONS are generally more differentiable within T2 weighted MRIs, the majority of the nerve becomes indistinguishable 6 mm posterior to the optic globe. T1 weighted scans consistently produced clarity at least 20 mm posterior to the optic globe. To accomplish tortuosity assessment only the ON center is needed. However, a severe ONS kink could influence the selection of the ON center. Because we did not observe any major kinks in all cases, we chose to use the T1 weighted MRI which allowed us to analyze a larger section of the ON.

This study introduces recovery scan analysis in order to assess ocular structural adaptations upon returning to a normal gravitation field. These scan times were set to certain ranges of days post-flight. The initial return time (R+1/3) is critical for detecting spaceflight

associated changes. This scan was conducted on average 4 ± 2 days after landing possibly allowing for redistribution of fluids. While there may be extensive protocols and health considerations that delay scan times, prompt MRI scanning would help to reduce time allowed for natural CSF and tissue recovery. Additionally, multiple pre-flight scans could allow for analysis of natural changes to the ON and ONS leading up to spaceflight. Given the average pre-flight scan used in this study was 508 ± 230 days, immediate pre-flight scans could possibly allow for a better analysis of the true effects of spaceflight.

While the present study uniquely analyzes a population of long-duration spaceflight astronauts, both with control and recovery data, inherently sample size was small. In total we analyzed 8 of 10 Ocular Health astronauts for tortuosity and 5 of 10 astronauts for changes in ON and ONS areas. Although small, this sample size with multiple recovery scan points is larger than any previous long-duration spaceflight astronaut studies. A larger population of astronauts would be beneficial possibly allowing for a statistically more relevant finding. Additionally, the rate of SANS occurrence may limit the power of findings in smaller groups of astronauts. However, long-duration spaceflight astronauts are a rare population making them difficult to study in large populations. These methods should be applied to larger groups in future studies.

Chapter 4: Automated MRI Based Quantification of Posterior Globe Deformation Recovery After Long-duration Spaceflight

Abstract

Ophthalmic changes have been both reported and observed in some astronauts as a result of extended stay in microgravity conditions. These changes are theorized to result from headward fluid shifts that cause elevated intracranial pressure within the cerebrospinal fluid space that surrounds the ON. A collection of symptoms associated with these changes has been defined as SANS and include disturbances to the ON, ONS, and the globe of the eye. Specifically, the posterior globe has been observed to flatten in some astronauts, causing vision problems as well as pain. While these changes often have been observed to resolve themselves upon return to Earth, extended spaceflights, such as the journey to Mars, will likely result in increased damage that may be irreversible. The present study aimed to provide reliable, quantitative analysis of posterior globe deformation in long-duration spaceflight astronauts. Automated methods were developed in order to map the posterior globe from pre- and post-flight MR images at five timepoints post-flight (R+1/3, R+30, R+90, R+180, and R+360). Average change in volumetric deformation for each time point with respect to the pre-flight scan were; 10.76 ± 11.93 mm^3, 9.24 ± 11.09 mm^3, 6.91 ± 8.95 mm^3, 2.57 ± 6.45 mm^3, and 7.30 ± 8.47 mm^3 respectively. As previously observed, a tendency for ocular structure adaptations to return to normal were generally observed for most individuals. Automated quantitative MRI based assessment of globe deformations could help our understanding of SANS and help assist in its prevention.

Introduction

SANS pathophysiology has been extensively investigated in long-duration spaceflight astronauts for many years. This condition impacts numerous ocular structures, including the posterior sclera. The rate of visual degradation reported by astronauts increases with spaceflight duration and about half of long-duration spaceflight astronauts report visual acuity changes that could be associated with a hyperopic shift[12,13,15]. A case study of one astronaut with globe flattening was described by Mader et al. in which spaceflight duration had a demonstrable effect[12]. Kramer et al. observed globe flattening in 7 of a 27 astronaut cohort[15]. In addition to globe flattening, choroidal folds and optic disc edema are commonly reported[12,13,15,18].

A leading hypothesis for the cause of globe flattening is a cephalad fluid shift during exposure to microgravity. Since communication exists between the intracranial and intraorbital cerebrospinal fluid (CSF) space, intracranial pressure (ICP) changes may result in a translaminar pressure gradient with intraocular pressure (IOP)[15]. Such a gradient could lead to susceptibility of the sclera to become indented. Swelling of the choroid may also significantly displace the aqueous humor independent of scleral flattening[12]. While the physiology of globe flattening in astronauts is not fully understood, similar structural changes have been observed in patients with idiopathic intracranial hypertension (IIH)[37-40]. These observations support that studies of the posterior sclera centered around the ON head are needed.

There have been a number of clinical assessments of globe flattening in astronaut and IIH subjects. Optical coherence tomography (OCT) is a commonly applied method for

structural assessment of the posterior globe. The use of magnetic resonance imaging (MRI) for the same purpose is less common, however, efforts have been made to establish a standard for its use in assessment of ocular anatomy. Jinkins et al. was able to identify ONH protrusion in 10 of 15 patients with high ICP using MRI[41]. Currently there are several proposed methods for performing MRI based three-dimensional modeling of the optic globe[37,42]. Applying similar methods to an astronaut cohort may help our understanding of SANS.

In this study, an automated method was developed to perform MRI based segmentation of the optic globe. This method was applied to 10 long-duration spaceflight astronauts and resulting segmentations were parameterized to compare posterior globe shape. Results were correlated with optical biometry measurements.

Methods

Study Participants

MRI data collection for this study was approved by the NASA and University of Idaho institutional review boards and satisfied all local and international regulations for human subject research. All data was de-identified before data transfer to the University of Idaho for analysis. 10 long-duration spaceflight astronauts from the Ocular Health study (NASA) were scanned pre-flight and post-flight. In both situations there were multiple timepoints at which scans were acquired. Timepoint labels were defined by the letters L and R, standing for launch and return, followed by a time range. Two pre-flight timepoints were defined in weeks prior to launch (L-9/6, L-21/18). 5 return timepoints were defined in days post-flight (R+1/3, R+30, R+90, R+180, and R+360). Multiple return timepoints allowed for quantification of posterior

globe recovery. 2 of the 10 astronauts completed both pre-flight timepoints. In all cases the pre-flight timepoint closest to the launch date was used to minimize the influence of natural changes occurring to ocular structures.

MRI Acquisition

T2 axial spin echo fat suppressed MRI sequences were collected using a 3T Siemens Verio scanner (Software ver. syngo MR B19, Munich, Germany) with 0.390 mm in plane isotropic pixel size (FOV 100 x 100), and 0.800 mm slice thickness and spacing. Additional sequence parameters included a 170° flip angle, repetition time (TR) 750 ms, echo time (TE) 111 ms, and pixel bandwidth 211 Hz/pixel.

MRI Reformatting

Each MRI orbit was radially resliced in Osirix (version 8.0.1, Pixmeo, Geneva, Switzerland) at one-degree increments (180 slices) about a central rotational axis (Figure 4.1 a). This created consistent intervoxel averaging of the scleral margin. The rotation axis was defined by manual selection of the ONH and lens center through which a view axis was aligned. The opposing ONH point was used to approximately align the first slice axially. Each slice was exported as a 16-bit image with 512 rows and columns with minimal padding around the globe.

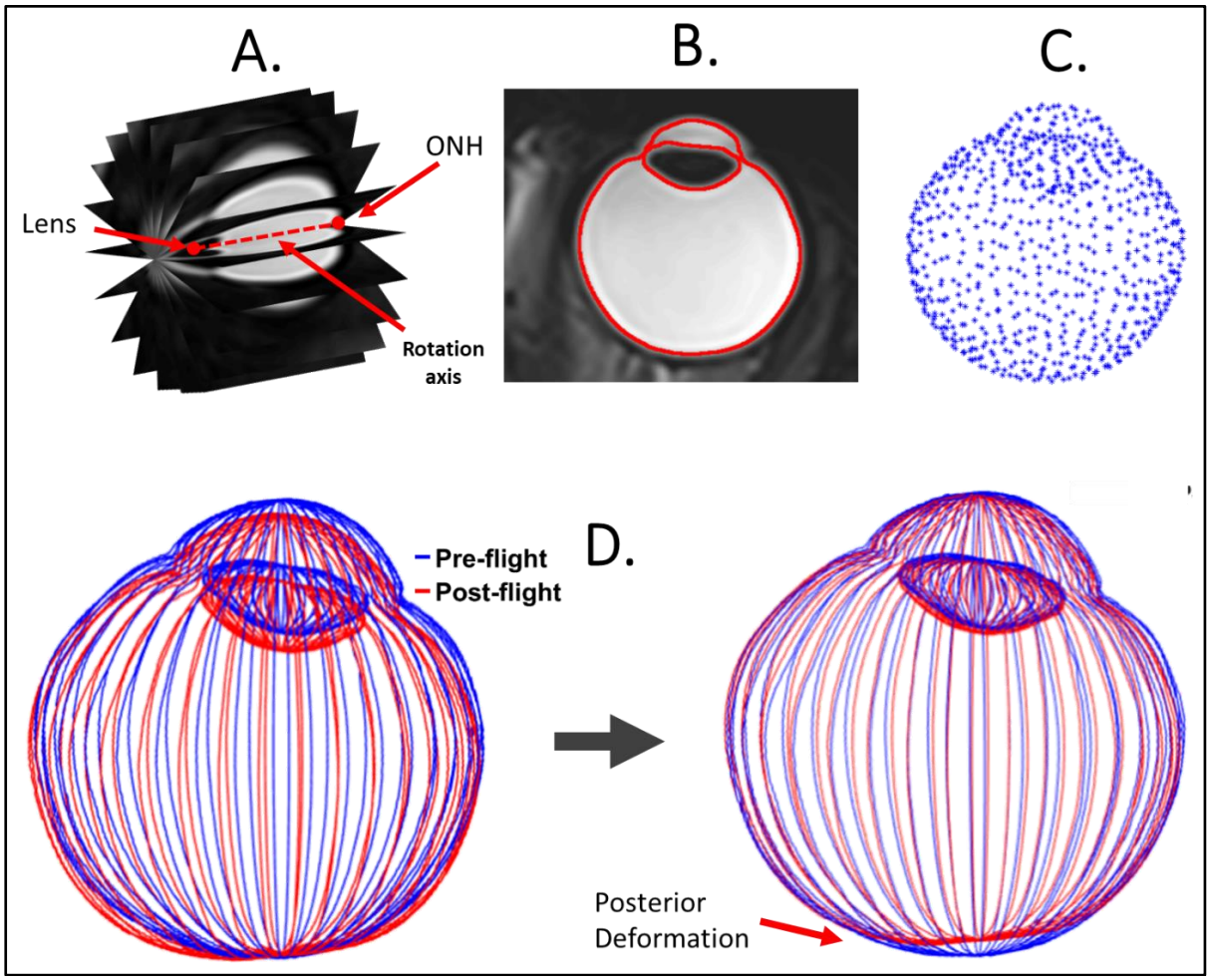

Figure 4.1. Methods for segmenting T2-weighted axial MRI including a) radial re-slicing, b) segmentation, c) 3D reconstructed down sampled point cloud, and d) registration of point clouds.

Point Cloud Generation

3D reconstructions of each globe were created and mapped to a common coordinate system using a multistep process (Figure 4.1 a-d). Global thresholding was used to segment the optic globe. To account for variations in scan intensity, a histogram-based selection of background pixels was considered to compute a threshold offset. Each slice was cubically up sampled by a factor of 4 before applying a threshold value of 380 plus the predetermined offset for the respective scan. The initial threshold of 380 was chosen based on anatomical accuracy of the resulting geometries and maximization of the total number of analyzed

subjects. After thresholding, a flood fill operation was applied to preserve only the region of the globe. Next, the edge points of the globe were collected and transformed to 3D MRI coordinates. Every point cloud was down sampled using a box grid filter with a filter size of 0.5 to ensure that the points were uniformly spaced. The down sampled point clouds were then used in an alignment process. This process involved choosing a pre-flight point cloud as a baseline and registering each subsequent point cloud using an iterative closest point algorithm with 60 iterations.

Deformation Map Generation

Deformation maps were generated to visualize posterior globe changes. First, the centroid for every eye was defined by averaging the locations of all points in the down sampled pre-flight point cloud. Next, an orientation vector scheme was created by the normal vector of the manually defined axial slice and the axis joining the ONH to the centroid, respectively. Using these two orientation vectors, a circumferential and meridional coordinate system was created based on Grytz et al.[43]. The points of each globe were then converted to polar coordinates where circumferential and meridional angles were transformed into angular and radial coordinates, respectively. These points were interpolated onto a square grid to allow for pairwise comparison between the pre- and post-flight distance maps (Figure 4.2). The length of each vector was represented by a color ranging from red to blue, for longer to shorter distances. A subtraction (post-flight - pre-flight) was performed to create a deformation map of the posterior globe (Figure 4.2). Only the region within a 4 mm radius

from the ONH was quantified. Two parameters, volume deformation and mean deformation, were computed based on these maps.

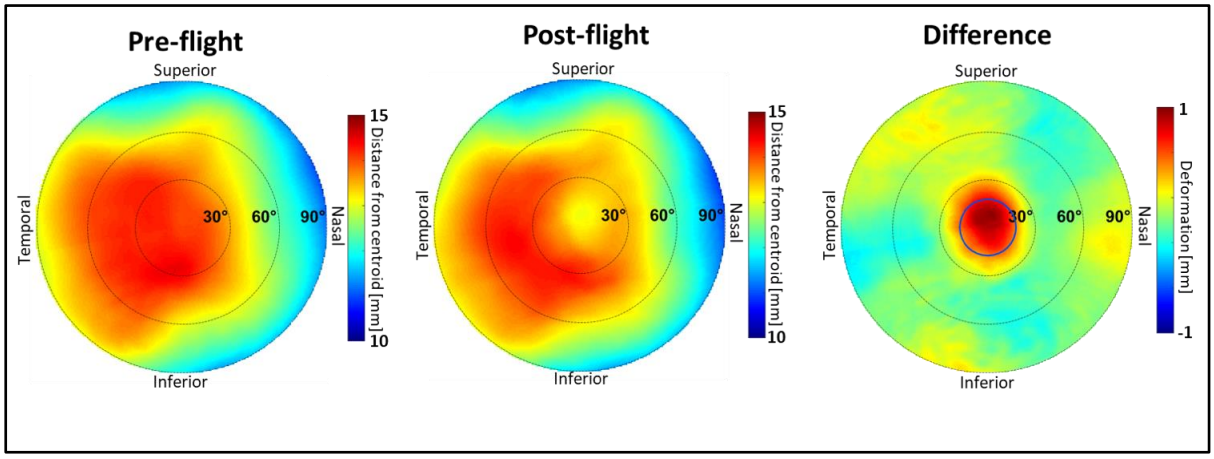

Figure 4.2. Example pre- and post-flight distance maps and resulting deformation map for the posterior surface of one eye with notable globe flattening. 4mm region is highlighted (blue) on the deformation map.

Statistics

Descriptive statistics were performed to calculate mean and standard deviation of the change in each parameter pre- to post-flight. A Bland-Altman plot was generated set to a 95% confidence interval to compare the gold standard optical biometry measurement with mean deformation values. Limited subject numbers did not allow analysis by sex.

Results

Study Population

Globe deformation was quantified in all 10 astronauts at one or more post-flight timepoints. Due to MRI intensity inhomogeneity, gradient, and movement artifacts, some timepoints from different subjects were excluded from the analysis. The average age was 42.9

± 5.6 years, body mass index 24.0 ± 1.8, and flight duration 167 ± 17 days (Table 4.1). Average scan timepoints for this group included: launch average (508 ± 230 days), R+1/3 (4 ± 2 days), R+30 (31 ± 5 days), R+90 (101 ± 16 days), R+180 (188 ± 15), and 360 days (355 ± 14 days).

Table 4.1. Average change and standard deviation in each parameter by scan time.

Parameter	Launch	R+1/3	R+30	R+90	R+180	R+360
Volume Deformation (mm^3)	n/a	10.76 ± 11.93	9.24 + 11.09	6.91 ± 8.95	2.57 ± 6.45	7.30 ± 8.47
Delta Optical Biometry (mm)	n/a	-0.12 ± 0.13	-0.09 ± 0.12	-0.08 ± 0.10	-0.78 ± 0.10	-0.07 ± 0.10
Mean Deformation	n/a	0.21 ± 0.23	0.18 ± 0.22	0.13 ± 0.17	0.05 ± 0.13	0.14 ± 0.17
N, Eyes	n/a	9, 17	9, 18	10, 18	7, 12	7, 13
Scan Time (days)	508 ± 230	4 ± 2	31 ± 5	101 ± 16	188 ± 15	355 ± 14

Globe Deformation

Posterior globe deformation was mapped and quantified in all 10 long-duration spaceflight astronauts (n = 20 eyes) at one or more of the return time points (Figure 4.3). Nearly all subjects exhibited some degree of globe flattening, represented by a positive volume deformation (red). Notably, the subject with the greatest degree of volume deformation (22.43 and 39.16 mm^3 for the left and right eyes), was clinically diagnosed with SANS. This individual exhibited grade 1 optic disc edema via fundus imaging (Subject 2).

Figure 4.3. Summary of all globe deformations within a 4 mm radius around the ONH at multiple time points post-flight (R+1/3, R+30, R+90, R+180, R+360). Ocular sinister (OD) and ocular dextrus (OD) refer to left and right eye respectively.

Nearly all subjects that showed initial positive globe deformation post-flight reduced over time (Figure 4.4 a, b). The globe deformation measurements also exhibited a strong correlation with optical biometry gold standard measures (R^2 = 0.6186). The mean volume deformation measured immediately after return (R+1/3) was 10.76 ± 11.93 mm^3 (Table 4.1). For the recovery time-points, mean volume deformation was 9.24 ± 11.09 mm^3 (R+30), 6.91 ± 8.95 mm^3 (R+90), 2.57 ± 6.45 mm^3 (R+180), and 7.30 ± 8.47 mm^3 (R+360). Average change in optical biometry acquired axial length for each post-flight timepoint was -0.12 ± 0.13 mm

(R+1/3), -0.09 ± 0.12 mm (R+30), -0.08 ± 0.10 mm (R+90), -0.78 ± 0.10 mm (R+180), and -0.07 ± 0.10 mm (R+360). The average value of the mean deformation parameter at each timepoint was 0.21 ± 0.23 mm (R+1/3), 0.18 ± 0.22 mm (R+30), 0.13 ± 0.17 mm (R+90), 0.05 ± 0.13 mm, (R+180), and 0.14 ± 0.17 mm (R+360). The average difference between change in optical biometry axial length and mean deformation was 0.045 ± 0.124 mm and linear correlation yielded an R^2 of 0.6236 (Figure 4.4 c). The Bland-Altman plot (Figure 4.4 d) shows agreement between these variables with the majority of the data points lying within the 95% confidence range.

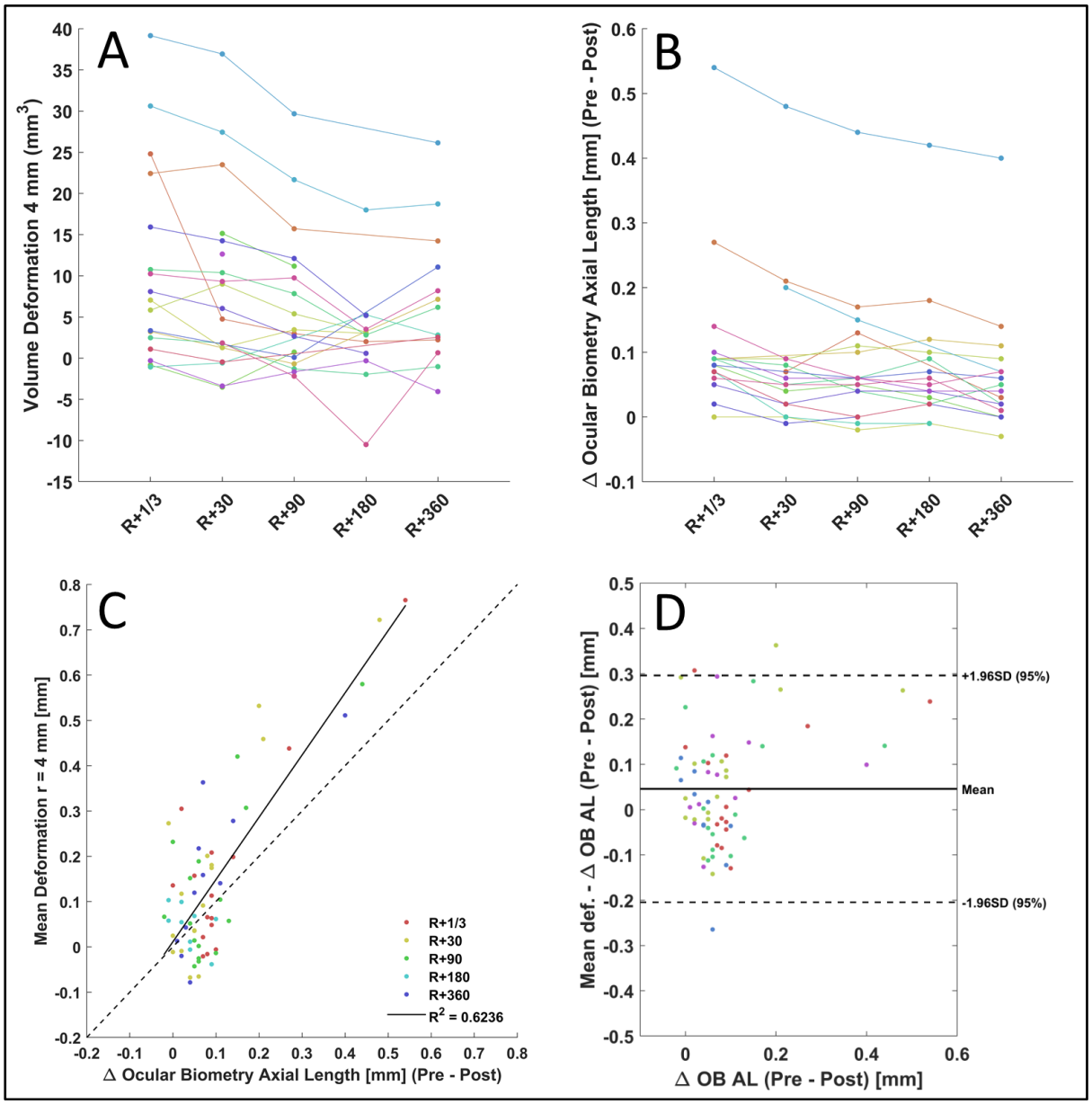

Figure 4.4. Plots showing volume deformation values and ocular biometry changes at all post-flight time points (a, b). Volume deformation was linearized as a mean value and compared with ocular biometry changes using correlation and Bland-Altman plots (c, d).

Discussion

Objective MRI-based volumetric quantification of posterior sclera morphometric changes lends support to previous findings of globe flattening and optic disc edema in astronauts[12,14,15] . As far as we know, this is the first study to objectively quantify globe

flattening in long-duration spaceflight astronauts in the context of post-flight recovery. Our findings suggest that pathological globe flattening is not widespread. However, there is a consistent trend of small, inward displacements of the vitreoretinal interface after exposure to microgravity in all subjects. These changes tended to decrease over time after return to earth but did not fully recover one-year post-flight. The exhibited recovery may provide a metric for potential effectiveness of countermeasures after deformation occurs. Optical biometry measurements provided a relative gold standard to compare to and suggest that the deformation parameters described accurately represent posterior globe changes.

Recovery of Deformation and Relation to SANS

The inclusion of multiple post-flight recovery timepoints in the current study provides a unique quantitative assessment of SANS induced globe flattening. There is an identifiable association between the magnitude of the deformation parameter and duration of time after spaceflight. In general, the highest degree of deformation was present immediately post-flight and gradual unresolved recovery occurred over the following year. Since the applied segmentation methods are limited to detecting the inner scleral margin, the deformation parameter is linked to morphometric changes beyond purely inward movement of the sclera proper. Therefore, the deformation parameter should be thought of as globe flattening in combination with choroidal swelling, retinal nerve fiber layer thickening, and optic disc edema. However, there is a presumable threshold at which the deformation exhibited exceeds the maximum possible change in total scleral thickness. This is important context when

examining recovery in the deformation parameter and making comparisons to previous astronaut studies.

Comparison to Studies in Astronauts

There have been several clinical ocular examinations of long-duration spaceflight astronauts reported. Mader et al. identified globe flattening and optic disc edema in 5 of 7 long-duration spaceflight astronauts and retinal nerve fiber layer thickening in 6[12]. In 2017, Mader et al. published a case report of an astronaut who developed asymmetric optic disc swelling. Total retinal thickness peaked in space and decreased after return with the right eye unresolved 630 days post-flight[14]. MRI-based clinical reporting by Kramer et al. revealed globe flattening in 7 of 27 astronauts[15]. In comparison, two astronauts in the current study exhibited degrees of deformation (> 500 µm) extensive enough to be directly linked with globe flattening. The average thickness of the retinal nerve fiber layer and choroid for normal eyes was 85.8 µm[44] and 272 µm[45] respectively, which together is much less than the extensive deformation previously reported.

MRI Based Optic Globe Quantification in Previous Studies

Semi-automated MRI-based mapping of the optic globe has been performed previously in several studies. These methods are summarized in Table 4.2. Each study produced differing parametrizations of the optic globe that could allow for pair wise comparisons. These parameterizations require developing a coordinate system that is dependent on anatomical reference points. Across these studies this was accomplished with registration, the definition

of anatomical axis, or a combination of the two. We used an ICP algorithm with a least squares metric to minimize the differences between matching point clouds. This is a conservative approach since all points are weighted equally. Performing registration after segmentation avoids the difficulty of aligning the unanchored globe in MRI at the cost of possible error introduced from segmentation artifacts and loss of volumetric information. Fairness of the registration was dependent on point cloud uniformity, which was accounted for with a box-grid filter. Our segmentation was aided by the radially resliced MRI orbit to obtain consistent inter-voxel averaging of the edge of the globe. This highly automated registration method in combination with the unique multi-timepoint study design adds strength to the current study.

Optical Biometry and Method Reliability

Optical biometry measurements are the gold standard of optical measurements in the medical community today. This technique utilizes infrared light to measure the anatomy of the eye with high accuracy. Axial length is the standard measurement for defining the distance from the corneal surface to the retinal surface. In the astronaut population calculating the difference between pre- and post-flight axial length offers a simple one-dimensional value for globe flattening. This, like the deformation variable, does not account for individual posterior globe layer changes (retina, choroid, and sclera). However, this offers an accepted medical measurement to which the deformation variable can be correlated. Additionally, the mean deformation parameter is based on regional assessment around the ON head while axial length is measured along the central axis of the eye (cornea to fovea). This introduces a

minimal change in axial length, when compared to axial length parameter, but still offers a notable comparison of change in posterior globe flattening.

Globe Flattening Pathology

The mechanisms underlying the development of globe flattening is likely due to many factors. Understanding how each of these mechanisms may play a role in astronauts will assist the interpretation of present findings. Because only a subset of astronauts have been clinically diagnosed with globe flattening, there may be physiological predispositions related to its development. Likely mechanisms may be identified through the lens of ocular structural physiology and terrestrially pathologies, each of which are discussed in detail.

The sclera plays a critical role in the structural integrity of the eye and in abnormal states may be susceptible to ocular hypertension and CSF pressure changes. Glaucoma patients were found to have thinner posterior scleral walls indicating a susceptibility to increased IOP[46]. In normal eyes, scleral thickness is greatest in the posterior pole of the globe and regions surrounding the ONH[46,47]. This causes some skepticism as to the ability of the sclera to be deformed by perineural forces – especially if ICP is not pathologically elevated. This could indicate that the risk of globe flattening is partly defined by structural predispositions in the sclera. IOP is an important component of structural adaptability of the eye and should not be discounted in this discussion. Previous work has demonstrated the compensatory effect of IOP and the potential to manage structural degradation of the sclera and ONH by controlling pressure levels[48].

Many potential posterior changes in the globe do not necessitate restructuring of the sclera. Choroidal expansion and retinal thickness may contribute to small, vitreoretinal interface displacements as opposed to scleral remodeling alone. Nearly all subjects in the current study demonstrated some recovery from immediate post-flight values. If choroidal expansion is represented by small volume deformations, then the choroid shows at least some ability to recover after spaceflight. Previous measures of choroidal changes in long-duration spaceflight astronauts indicate a potential for hyperopic related visual degradation[49]. Remodeling of the various layers of the sclera, however, do not explain the large deformations observed in SANS diagnosed subjects.

The ON may play a critical role in ICP related factors that contribute to globe flattening. The ONS is known to be sensitive to pressure changes until a saturation point is reached wherein increases in CSF pressures no longer result in ONS diameter changes[31,50]. Previous studies found the saturation point to be predictive of ocular damage and lower saturation points in some people may exacerbate perineurial forces on the ONH and globe[50,51]. Kramer et al. reported a link between larger ONS diameters and globe flattening[15].

IIH is often discussed in the context of SANS due to the observation of ONS distention and globe flattening in both disorders. There is reason to believe that elevated intraorbital CSF pressure is an important factor in the development of globe flattening in astronauts[38]. Unlike bilateral globe flattening in IIH however, globe flattening in SANS is often asymmetric[12]. In the current study, the two most affected subjects exhibited more globe flattening in the right eye compared to the left. Due to this dissimilarity, it cannot be concluded that IIH is analogous to SANS.

Limitations

The study population of (n = 10) astronauts does not allow for strong statistical analysis. This is the nature of astronaut studies however, as it is inherently a small population specifically when referring to long-duration spaceflight. This study has a larger sample size compared to previous studies analyzing long-duration spaceflight astronauts.

Due to either a lack in scan quality or missing data we had to throw out 22 eyes from our assessment. Some of the artifacts found in scans of bad quality were limited to one eye, such as a "shadow" or a missing edge. Motion artifacts also occurred in some scans causing both eyes to be thrown out. Ultimately, the majority of scans were kept for analysis (78 eyes).

While MRI provides the opportunity to examine orbital anatomy in high resolution and 3 dimensions, there is no scanner on the ISS restricting these types of studies to terrestrial environments. The only ophthalmic imaging device the astronauts used while in microgravity is ultrasound due to its minimal size and energy requirements. However, this tool requires precise measuring techniques that usually develop in specialist of years. Astronauts do not receive such training and are therefore liable to cause measurement errors. Because of this research, like the present study, lacks data from the inflight mission time period. While analyzing the immediate post-flight scan should give some indication of the ophthalmic changes that have occurred, we cannot be completely sure these changes have not already recovered to some extent.

This study includes a novel recovery scan analysis for long-duration spaceflight astronauts that consist of five postflight scans spanning one year. These scans were defined by a range of time after return. The initial return time (R+1/3) is the most crucial return scan

time because it most closely highlights the ophthalmic changes that may have occurred during spaceflight. On average this scan was conducted 4 ± 2 days after return to Earth across all astronauts. Earlier scan times would allow for a better analysis of spaceflight induced disturbances.

Due to inherent challenges in MRI acquisition and segmentation, artifactual differences in the cornea and lens were common. This required subjective assessment of geometric agreement between point clouds. Due to the nature of the study, we could not control for previous space-flight exposure and G-forces related to pre-flight training.

Table 4.2. Comparison of segmenting and parameterization techniques for posterior globe analysis across various studies.

Method	MRI Protocol	Relevant Outcomes	Citation
Segmentation Expectation-maximization **Parameterization** Axial plane matching with rigid linear MRI registration; Orthogonal coordinate system w.r.t axis formed by lens center to globe center of mass.	1.5/3T T2 3D CISS: 0.6 mm in plane isotropic; slice thickness, 0.6 mm; TR, 6.35/5.42 ms; TE, 2.82/2.43 ms; flip angle, 47/34°; pixel bandwidth, 560/650 Hz/pixel	2D cartesian deformation map and corresponding measures: nerve protrusion (NP), globe flattening (GF), maximum deformation (MD) Control, IIH mean ± SD measures, respectively: NP 0.96 ± 0.013, 0.91 ± 0.028, p = .00002 GF 0.93 ± 0.020, 0.91 ± 0.022, p = .0035 MD 0.93 ± 0.021, 0.88 ± 0.027, p = .00002	Alperin et al.
Segmentation Flood fill and morphology **Parameterization** Conic projection based on conic axis defined by lens center to center of vitreous body.	T1 3D inversion recovery turbo gradient echo: 0.5 mm in plane isotropic (FOV 40 x 46 mm); slice thickness, 1mm; TR, 2.5 ms; TE, 4.55 ms; flip angle, 16°; inversion time, 1280 ms;	Circular retinal distance map MRI vs PCI axial length mean ± SD difference: 0.08 ± 0.23 mm p = 0.01 MRI intersession retinal map standard deviation = 0.11 mm (4 subjects, scanned twice) Does not account for patient orientation changes	Beenakker et al.
Segmentation Flood fill followed by spherical mesh shrink-wrap and local averaging. **Parameterization** Circumferential w.r.t axial length	T2 half-acquisition turbo spin-echo sequence: 0.5 mm place isotropic (FOV, 256 x 256 mm); 1 mm slice thickness; TR, 1240 ms; TE, 124 ms; flip angle, 150°; 6 averages; 4/8 partial-phase acquisition	Circumferential color-coding w.r.t axial length Axial length intersession repeatability (one subject, 10 scans) mean ± SD: Right eye = 23.78 ± 0.27 mm Left = 24.41 ± 0.52 mm	Singh et al.
Segmentation Intensity offset global thresholding **Parameterization** Iterative closest point registration; circumferential and meridional coordinate system.	T2 axial spin echo fat suppressed MRI: 0.390 mm in plane isotropic (FOV, 100 x 100); 0.800 mm slice thickness and spacing; TR, 750 ms; TE 111 ms; flip angle, 170°; pixel bandwidth, 211 Hz/pixel .	2D polar deformation map Mean deformation moderately correlated with change in optical biometry axial length: R^2 = 0.624. Mean difference between change optical biometry axial length and mean deformation: 0.045 ± 0.124 mm. Not dependent on patient orientation	Current study.

Chapter 5: Project Research Outputs

Below is a list of grants secured for or due to this project. Additionally, a list of documents that were generated utilizing this research are reported.

Grants Secured

NASA - Ophthalmic and Intracranial Structural Changes in Head-down Tilt Bedrest: Potential Countermeasures and Comparison to SANS Findings in Astronauts (Co-Investigator: Bryn A. Martin PhD, Principal Investigator: Brandon Macias PhD)

10/01/2020-9/30/23 (exact dates TBD), The purpose of this study is to determine if ophthalmic and intracranial structural alterations are similar in prolonged 6° HDT bed rest compared to long-duration astronauts with SANS and to determine if these alterations will be reduced by countermeasures applied during bed-rest.

Idaho Space Grant Consortium Graduate Student Fellowship (Mentor: Bryn A. Martin, PhD, Recipient: Jesse Rohr)

6/1/2017-5/30/2018, Idaho Space Grant Consortium, NASA Prime Grant No. NNX15AI04H (PI Law J): The purpose of this project is to mentor a graduate student in conducting research.

Idaho Space Grant Consortium Undergraduate Student Fellowship (Mentor: Bryn A. Martin, PhD, Recipient: Austin Sass)

6/1/2017-5/30/2018, Idaho Space Grant Consortium, NASA Prime Grant No. NNX15AI04H (PI Law J): The purpose of this project is to mentor an undergraduate student in conducting research.

Prospective Observational Study of Ocular Health in Crews (Ocular Health Study) (Co-Investigator: Bryn A. Martin PhD, Principal Investigator: Brandon Macias PhD)

5/4/2015-9/30/2019, The purpose of this study is to collect evidence to characterize the risk and define the visual changes, vascular changes, and central nervous system (CNS) changes, including intracranial pressure, observed during long-duration exposure to microgravity, including postflight time course for recovery to baseline. This study gathers information that can be used to assess the risk of Microgravity-Induced Visual Impairment/Intracranial Pressure (VIIP) and guide future research needs.

Fluid Distribution before, during and after Prolonged Space Flight (Fluid Shifts Study) (Co-Investigator: Bryn A. Martin PhD, Principle Investigator: Drs. Michael Stenger, Scott Dulchavsky, Alan R. Hargens)

5/4/2015-9/30/2020, The purpose of this study is to characterize fluid distribution and compartmentalization associated with long-duration space flight, and to correlate these findings with vision changes and other elements of the SANS syndrome

Advanced Ocular and Brain MRI of Astronauts Following Long Duration Space Flight (Principal Investigator: Bryn A. Martin, PhD);

5/1/2016-4/30/2018, Idaho Space Grant Consortium, NASA Prime Grant No. NNX15AI04H (PI Law J): The purpose of this study is to develop and apply tools to quantify optic nerve tortuosity and 3D structure in long-duration space flight astronauts.

Simulations of CSF, Hemodynamics and Ocular Risk (VIIP SCHOLAR) (Co-Investigator: Bryn A. Martin, PhD);

10/01/2016-9/30/2019, National Space Biomedical Research Institute, NNX16AT06G: The purpose of this study is to develop tools to compute CSF fluid shifts in microgravity and the effect on the eye using a combination of advanced medical imaging and computational modeling tools.

Abstracts Published

Martin BA, Rohr JJ, Sass A, Sater S, Macias B, Stenger M, "Magnetic Resonance Imaging Quantification of Ophthalmic Changes Due to Space Flight," 2019 NASA Human Research Program / IWS (Galveston, TX, January 23, 2019).

Rohr JJ, Sass AM, Sater S, Macias B, Oshinski JN, Ethier CR, Stenger M, Martin BA, "MRI-based quantification of optic nerve tortuosity and subarachnoid space 3d geometry: reliability assessment," NASA Human Research Investigator's Workshop (Galveston, TX, 1/22-25/2018).

Rohr JJ, Sass AM, Stenger M, Macias B, Ethier CR, Sargsyan AE, Martin BA, "Automated Method to Quantify 3D Geometric Alterations of the Optic Nerve and Sheath in Astronauts," NASA

Human Research Program Investigators' Workshop, The Gateway to Mars (Galveston, TX, 1/22-25, 2018).

Macias BR, Otto C, Patel N, Kramer L, Martin BA, Ploutz-Snyder R, Sargsyan A, Alexander D, Riascos R, Samuels B, Gibson C, Lee S, Laurie S, Marshall-Goebel K, Stenger M, "Ocular Health" 2019 NASA Human Research Program / IWS (Galveston, TX, January 23, 2019).

Rohr JJ, Sass AM, Sater S, Aldrimk B, Stenger M, Macias B, Ethier CR, Sargsyan A, Martin BA, "Inter-operator Reliability Assessment of Optic Nerve Tortuosity in Long-duration Flight Astronauts," 33rd Annual Meeting of the American Society for Gravitational and Space Research (Seattle, WA, 10/25-28/2017).

Sass AM, Sater S, Rohr JJ, Macias B, Oshinski JN, Ethier CR, Stenger M, Martin BA, "Methods for Quantifying Tortuosity and 3D Geometry Changes Occurring to the Optic Nerve During Long-Duration Spaceflight," University of Idaho Undergraduate Research Symposium (Moscow, ID, 4/30, 2018).

Sater S, Sass A, Aldrimk B, Rohr JJ, Stenger M, Macias B, Martin BA, "Reliability assessment of Optic Nerve Trajectory in Long-duration Space Flight Astronauts," University of Idaho, Undergraduate Student Research Symposium (Moscow, ID, 4/24, 2017).

Ethier CR, Myers JG, Nelson E, Martin BA, Oshinski JN, Samuels B, Feola AJ, “Effects of CSF pressure on the eye: a computational-experimental comparison,” NASA Human Research Investigator’s Workshop (Galveston, TX, 1/22-25/2018).

Nelson ES, Myers JG, Lewandowski B, Feola AJ, Werner C, Raykin J, Martin BA, Samuels B, Ethier CR, “Ocular modeling for VIIP syndrome: how experimental and numerical studies can collaborate,” NASA HRP Investigators Workshop (Galveston, TX, 1/24, 2017).

Lee C, Rohr JJ, Sass A, Sater S, Martin BA, Zahid A, Oshinski J, Ethier CR, “In Vivo Estimation of Optic Nerve Sheath Stiffness Using Noninvasive MRI Measurements and Finite Element Modeling,” Summer Bioengineering, Biotransport, and Biomechanics Conference, SB^3C (Seven Springs, PA, 6/25-28, 2019).

Martin BA, Rohr JJ, Sass A, Sater S, Oshinski J, Ethier C, Lee C, “Non-Invasive Quantification of Optic Nerve and Sheath Geometric Changes and Mechanical Properties by Head-Down Tilt Magnetic Resonance Imaging,” 2019 NASA Human Research Program / IWS (Galveston, TX, January 23, 2019).

Chapter 6: Conclusion

Summary of Findings

Specific Aims

The Specific Aims listed for this project were as follows:

Specific Aim 1

To quantify pre-flight ocular biomechanics in astronauts (n=10). This aim will allow us to understand the baseline variability in ocular biomechanics among an astronaut-like population.

Specific Aim 2

To quantify immediate post-flight ocular biomechanics in astronauts (n=10) and determine if measures of ocular biomechanics are altered due to space flight. This aim will allow us to test the hypothesis that space flight will result in a) Engorgement of the ocular nerve sheath subarachnoid space 3D geometry, b) Increase in ocular nerve tortuosity, c) Increase in ocular globe volumetric deformation (posterior globe flattening).

Specific Aim 3

To quantify recovery of ocular biomechanics in astronauts (n = 10) at five intervals over a one-year period after return from long-duration spaceflight missions.

In general, we did not observe ophthalmic changes outside parameter reliability in Tortuosity, ON area, and ONS area parameters while volumetric globe deformation was confirmed in many. A complete list of project results and implications are listed in Table 6.1. Because ON kinking has been reported in multiple astronaut studies, we did expect to quantify a change for this population. However, many of the previous studies did not have a baseline observation indicating that these ON kinks may have existed prior to flight. We did expect ON cross-sectional area to remain unchanged. While many subjects exhibited minimal reduction in size, often near the measurement reliability, one outlier exhibited a major increase in ON area. A lack in ONS cross-sectional area was the most surprising finding we reported as nearly all astronaut studies report ONS distension even on shorter missions. While immediate post-flight scans (R+1/3) were conducted during the first week of the astronauts return to Earth there is still a possibility that any ONS distension could rapidly recover prior to these scans. As predicted, volumetric globe deformation was observed in most subjects in this study. Recovery scans also indicated a natural trend toward baseline though many did not fully recover in the one-year period observed.

Table 6.1 Summary of project results and implications

Parameter	Result	Implications
ON Tortuosity (mm)	We did not observe the expected increase in kinking of ON in the astronaut population pre- to post-flight. • Average change R+1/3: -0.06 ± 0.42 (-0.9%) • Recovery measurements showed consistency of measurement technique.	ON tortuosity does not appear to be a common occurrence in this population of long-duration spaceflight astronauts. • Previous findings by researchers did not have baseline observation or measurement. • Also, they lacked quantitative measurement of tortuosity.
ON Cross-sectional Area (mm^2)	We did not observe ON cross-sectional area change as expected. Subtle decreases were observed with one major increase • Average change R+1/3: 0.58 ± 2.53 (6.7%) • These changes were generally minimal thus recovery was not notably observed. • Measurement values were near the measurement reliability	• ON inflammation has not been previously documented in astronauts. • These findings should be investigated in a larger cohort to confirm whether these changes are consistent
ONS Cross-sectional Area (mm^2)	ONS cross-sectional area showed no trend of change pre- to post-flight in the astronaut population. • Average change R+1/3: -0.88 ± 2.35 (-3.1%) • Recovery data showed consistent values across the timepoints in all individuals	This surprising finding potentially conflicts with the idea that ICP is elevated in space. • Need tools to assess ICP to confirm • Parameter may have rapidly returned to normal after return to Earth
Volumetric Globe Deformation (mm^3)	Volumetric Deformation was observed in most subjects in the astronaut population though only severe in two. • Average change R+1/3: 10.76 ± 11.93 • Recovery data highlighted a general trend of globe deformation returning to baseline. Many did not completely recover in the one-year period.	The presented novel parameter for volumetric globe deformation was found to be relevant in nearly all astronaut cases. • Single astronaut with SANS had much greater degree of volumetric glove deformation • Need larger cohort to determine if this parameter is related to SANS development. • Need to understand what eye structures are leading to volumetric deformation

Overarching conclusion

While changes were not often observed in this population of long-duration astronauts, we have produced a verified method to quantify ophthalmic structures. These measurements are novel and have been developed with automation in mind in order to reduce measurement error. We conducted a reliability study for any manual input required as well as developed phantom models to validate our method. These studies have given strength to the developed methods and allow for improved measuring standards for future work. These findings help provide basic information about how eye changes in astronauts and may help to identify SANS development in the astronaut population.

Future work

An optic globe phantom containing a set of globes and ON/ONS geometries has been produced. Upon receiving the associated MRI sequences, we will conduct the final phantom reliability assessment. The validation of the volumetric globe deformation parameter may allow for an integral technique to reliably quantify and diagnosing SANS in astronauts

These methods should be applied in more astronaut studies. Utilizing the techniques reported in this study may allow for a better understanding of the pathology of SANS development. Additionally, utilizing recovery analysis in more studies should help to better understand the underlying mechanisms related to SANS symptom development. Inclusion of mid-flight measurements would provide further understanding to the ophthalmic changes experienced by astronauts during spaceflight.

In addition to astronaut studies, these methods should also be applied to head-down tilt bed rest studies. This Earth based analogue for microgravity induced headward fluid shifts is yet to be accepted as an appropriate model for SANS development. Utilizing these techniques may help in quantifying ophthalmic structural changes in healthy subjects and correlating these changes to astronaut studies.

We ultimately want to allow for the production of successful countermeasures that will alleviate the symptoms of SANS in astronauts. It is our hope that these methods may provide the means necessary to further understand this syndrome.

References

1 *HRP Integrated Path to Risk Reduction*, <https://humanresearchroadmap.nasa.gov/intro/> (2018).

2 Michel, E. L., Johnston, R. S. & Dietlein, L. F. Biomedical results of the Skylab Program. *Life Sci Space Res* **14**, 3-18 (1976).

3 Muscle Atrophy. *NASA Information*. <https://www.nasa.gov/pdf/64249main_ffs_factsheets_hbp_atrophy.pdf>.

4 Cucinotta, F. A. Risk of Radiation Carcinogenesis. (NASA Johnson Space Center, Houston, TX, 2009).

5 Schauer, D. A. & Linton, O. W. NCRP Report No. 160, Ionizing Radiation Exposure of the Population of the United States, medical exposure--are we doing less with more, and is there a role for health physicists? *Health Phys* **97**, 1-5, doi:10.1097/01.HP.0000356672.44380.b7 (2009).

6 Abadi, L. J., LLoyd, C. W. & Shelhamer, M. J. The Human Body in Space. *Human Research Program*. <https://www.nasa.gov/hrp/bodyinspace>.

7 Antonutto, G. & di Prampero, P. E. Cardiovascular deconditioning in microgravity: some possible countermeasures. *Eur J Appl Physiol* **90**, 283-291, doi:10.1007/s00421-003-0884-5 (2003).

8 Zhang, L. F. & Hargens, A. R. Spaceflight-Induced Intracranial Hypertension and Visual Impairment: Pathophysiology and Countermeasures. *Physiol Rev* **98**, 59-87, doi:10.1152/physrev.00017.2016 (2018).

9 Roberts, D. R. *et al.* Effects of Spaceflight on Astronaut Brain Structure as Indicated on MRI. *N Engl J Med* **377**, 1746-1753, doi:10.1056/NEJMoa1705129 (2017).

10 Riascos, R. F. *et al.* Longitudinal Analysis of Quantitative Brain MRI in Astronauts Following Microgravity Exposure. *J Neuroimaging* **29**, 323-330, doi:10.1111/jon.12609 (2019).

11 Killer, H. E., Laeng, H. R., Flammer, J. & Groscurth, P. Architecture of arachnoid trabeculae, pillars, and septa in the subarachnoid space of the human optic nerve:

anatomy and clinical considerations. *Br J Ophthalmol* **87**, 777-781, doi:10.1136/bjo.87.6.777 (2003).

12 Mader, T. H. *et al.* Optic disc edema, globe flattening, choroidal folds, and hyperopic shifts observed in astronauts after long-duration space flight. *Ophthalmology* **118**, 2058-2069, doi:10.1016/j.ophtha.2011.06.021 (2011).

13 Mader, T. H. *et al.* Persistent Asymmetric Optic Disc Swelling After Long-Duration Space Flight: Implications for Pathogenesis. *J Neuroophthalmol* **37**, 133-139, doi:10.1097/WNO.0000000000000467 (2017).

14 Mader, T. H. *et al.* Optic disc edema in an astronaut after repeat long-duration space flight. *J Neuroophthalmol* **33**, 249-255, doi:10.1097/WNO.0b013e31829b41a6 (2013).

15 Kramer, L. A., Sargsyan, A. E., Hasan, K. M., Polk, J. D. & Hamilton, D. R. Orbital and intracranial effects of microgravity: findings at 3-T MR imaging. *Radiology* **263**, 819-827, doi:10.1148/radiol.12111986 (2012).

16 Marshall-Goebel, K. *et al.* Lower body negative pressure reduces optic nerve sheath diameter during head-down tilt. *J Appl Physiol (1985)* **123**, 1139-1144, doi:10.1152/japplphysiol.00256.2017 (2017).

17 Tavassoli, M. Medical problems of space flight. *Am J Med* **81**, 850-854 (1986).

18 Lee, A. G., Mader, T. H., Gibson, C. R., Brunstetter, T. J. & Tarver, W. J. Space flight-associated neuro-ocular syndrome (SANS). *Eye (Lond)* **32**, 1164-1167, doi:10.1038/s41433-018-0070-y (2018).

19 Marshall-Bowman, K., Barratt, M. R. & Gibson, C. R. Ophthalmic changes and increased intracranial pressure associated with long duration spaceflight: An emerging understanding. *Acta Astronautica* **87**, 77-87, doi:10.1016/j.actaastro.2013.01.014 (2013).

20 Lee, A. G. *et al.* Neuro-Ophthalmology of Space Flight. *J Neuroophthalmol* **36**, 85-91, doi:10.1097/WNO.0000000000000334 (2016).

21 Armstrong, G. T. *et al.* Defining optic nerve tortuosity. *AJNR Am J Neuroradiol* **28**, 666-671 (2007).

22 Campen, C. J. & Gutmann, D. H. Optic Pathway Gliomas in Neurofibromatosis Type 1. *J Child Neurol* **33**, 73-81, doi:10.1177/0883073817739509 (2018).

23 Jensen, R. H., Radojicic, A. & Yri, H. The diagnosis and management of idiopathic intracranial hypertension and the associated headache. *Ther Adv Neurol Disord* **9**, 317-326, doi:10.1177/1756285616635987 (2016).

24 Rigi, M., Almarzouqi, S. J., Morgan, M. L. & Lee, A. G. Papilledema: epidemiology, etiology, and clinical management. *Eye Brain* **7**, 47-57, doi:10.2147/EB.S69174 (2015).

25 Thurtell, M. J. & Wall, M. Idiopathic intracranial hypertension (pseudotumor cerebri): recognition, treatment, and ongoing management. *Curr Treat Options Neurol* **15**, 1-12, doi:10.1007/s11940-012-0207-4 (2013).

26 Roberts, D. R. *et al.* Structural Brain Changes following Long-Term 6 degrees Head-Down Tilt Bed Rest as an Analog for Spaceflight. *AJNR Am J Neuroradiol* **36**, 2048-2054, doi:10.3174/ajnr.A4406 (2015).

27 Taibbi, G. *et al.* Ocular Outcomes Comparison Between 14- and 70-Day Head-Down-Tilt Bed Rest. *Invest Ophthalmol Vis Sci* **57**, 495-501, doi:10.1167/iovs.15-18530 (2016).

28 Laurie, S. S. *et al.* Optic Disc Edema after 30 Days of Strict Head-down Tilt Bed Rest. *Ophthalmology* **126**, 467-468, doi:10.1016/j.ophtha.2018.09.042 (2019).

29 Rogowska, J. in *Handbook of Medical Image Processing and Analysis (Second Edition)* (ed Isaac N. Bankman) 73-90 (Academic Press, 2009).

30 Xie, X. *et al.* Noninvasive intracranial pressure estimation by orbital subarachnoid space measurement: the Beijing Intracranial and Intraocular Pressure (iCOP) study. *Crit Care* **17**, R162, doi:10.1186/cc12841 (2013).

31 Hansen, H. C. & Helmke, K. Validation of the optic nerve sheath response to changing cerebrospinal fluid pressure: ultrasound findings during intrathecal infusion tests. *J Neurosurg* **87**, 34-40, doi:10.3171/jns.1997.87.1.0034 (1997).

32 Sirek, A. S. *et al.* Doppler ultrasound of the central retinal artery in microgravity. *Aviat Space Environ Med* **85**, 3-8 (2014).

33 Wang, X. *et al.* Optic Nerve Tortuosity and Globe Proptosis in Normal and Glaucoma Subjects. *J Glaucoma*, doi:10.1097/IJG.0000000000001270 (2019).

34 Geeraerts, T. *et al.* Use of T2-weighted magnetic resonance imaging of the optic nerve sheath to detect raised intracranial pressure. *Crit Care* **12**, R114, doi:10.1186/cc7006 (2008).

35 Killer, H. E., Jaggi, G. P., Flammer, J., Miller, N. R. & Huber, A. R. The optic nerve: a new window into cerebrospinal fluid composition? *Brain* **129**, 1027-1030, doi:10.1093/brain/awl045 (2006).

36 Shinohara, R. T. *et al.* Corrigendum to "Statistical normalization techniques for magnetic resonance imaging" [NeuroImage: Clinical 6 (2014) 9-19]. *Neuroimage Clin* **7**, 848, doi:10.1016/j.nicl.2015.02.011 (2015).

37 Alperin, N., Bagci, A. M., Lam, B. L. & Sklar, E. Automated quantitation of the posterior scleral flattening and optic nerve protrusion by MRI in idiopathic intracranial hypertension. *AJNR Am J Neuroradiol* **34**, 2354-2359, doi:10.3174/ajnr.A3600 (2013).

38 Jacobson, D. M. Intracranial hypertension and the syndrome of acquired hyperopia with choroidal folds. *J Neuroophthalmol* **15**, 178-185 (1995).

39 Hingwala, D. R., Kesavadas, C., Thomas, B., Kapilamoorthy, T. R. & Sarma, P. S. Imaging signs in idiopathic intracranial hypertension: Are these signs seen in secondary intracranial hypertension too? *Ann Indian Acad Neurol* **16**, 229-233, doi:10.4103/0972-2327.112476 (2013).

40 Friedman, D. I. Idiopathic intracranial hypertension. *Curr Pain Headache Rep* **11**, 62-68 (2007).

41 Jinkins, J. R. *et al.* MR of optic papilla protrusion in patients with high intracranial pressure. *AJNR Am J Neuroradiol* **17**, 665-668 (1996).

42 Beenakker, J. W., Shamonin, D. P., Webb, A. G., Luyten, G. P. & Stoel, B. C. Automated retinal topographic maps measured with magnetic resonance imaging. *Invest Ophthalmol Vis Sci* **56**, 1033-1039, doi:10.1167/iovs.14-15161 (2015).

43 Grytz, R. *et al.* Material properties of the posterior human sclera. *J Mech Behav Biomed Mater* **29**, 602-617, doi:10.1016/j.jmbbm.2013.03.027 (2014).

44 Bowd, C., Weinreb, R. N., Williams, J. M. & Zangwill, L. M. The retinal nerve fiber layer thickness in ocular hypertensive, normal, and glaucomatous eyes with optical coherence tomography. *Arch Ophthalmol* **118**, 22-26, doi:10.1001/archopht.118.1.22 (2000).

45 Manjunath, V., Taha, M., Fujimoto, J. G. & Duker, J. S. Choroidal thickness in normal eyes measured using Cirrus HD optical coherence tomography. *Am J Ophthalmol* **150**, 325-329 e321, doi:10.1016/j.ajo.2010.04.018 (2010).

46 Norman, R. E. *et al.* Dimensions of the human sclera: Thickness measurement and regional changes with axial length. *Exp Eye Res* **90**, 277-284, doi:10.1016/j.exer.2009.11.001 (2010).

47 Vurgese, S., Panda-Jonas, S. & Jonas, J. B. Scleral thickness in human eyes. *PLoS One* **7**, e29692, doi:10.1371/journal.pone.0029692 (2012).

48 Sigal, I. A. & Ethier, C. R. Biomechanics of the optic nerve head. *Exp Eye Res* **88**, 799-807, doi:10.1016/j.exer.2009.02.003 (2009).

49 Patel, N., Pass, A., Mason, S., Gibson, C. R. & Otto, C. Optical Coherence Tomography Analysis of the Optic Nerve Head and Surrounding Structures in Long-Duration International Space Station Astronauts. *JAMA Ophthalmol* **136**, 193-200, doi:10.1001/jamaophthalmol.2017.6226 (2018).

50 Raykin, J. *et al.* Characterization of the mechanical behavior of the optic nerve sheath and its role in spaceflight-induced ophthalmic changes. *Biomech Model Mechanobiol* **16**, 33-43, doi:10.1007/s10237-016-0800-7 (2017).

51 Peter Wostyn, P. P. D. D. Optic Nerve Sheath Distention as a Protective Mechanism Against the Visual Impairment and Intracranial Pressure Syndrome in Astronauts. *ARVO* **58**, doi:10.1167/iovs.17-22600 (2017).